Telemark University College
Faculty of technology
M.Sc. Programme

MASTER THESIS 2008

Candidate : **Wenjun Wu**

Title : **Experimental study of bubbling fluidized bed**

Faculty of Technology
Address: Kjolnes Ring 56, N-3914 Porsgrunn, Norway, tel: +47 35 57 50 00, fax: +47 35 55 75 47

Telemark University College

Faculty of Technology

M.Sc. Programme

WRITTEN REPORT MASTER THESIS, COURSE CODE F4203

Student : Wenjun Wu

Thesis Title : **Experimental study of bubbling fluidized bed**

Signature :

Number of pages :

Keywords : bubbling fluidized bed, particle size distribution, minimum fluidization velocity, bubble velocity, bubble size

Supervisor : Britt M. Halvorsen sign.: . . . . . .

2nd Supervisor :

Sensor : J.Prieur du Plessis sign.: . . . . . .

Availability : Open

Archive approval : .. . . . . **Date:** . . . . . .

Abstract:

A series of experiments are performed in order to study the flow behaviour of bubbling fluidized bed. A two dimensional fluidized bed is built up with dimension 0.8 m (height) × 0.2 m (width) × 0.025 m (depth) and uniform porous gas distributor. Three powders with different particle size ranges are used in the experiments. The mean particle sizes are 153, 484 and 960 µm. The minimum fluidization velocities are measured for the three powders. The experiments are performed with different superficial velocities and with two different initial particle bed heights. According to experiments, the minimum fluidization velocity increases with increasing particle size. It is also observed that the size and the shape of the bubbles are strongly influenced by the particle size in the bed. The bubbles also change with the distance above the distributor. The bubble velocity increases with the height in the bed and with the inlet superficial gas velocity.

Emphasis is given to study the effect of particle size distribution on flow behaviour in bubbling fluidized beds.
Experiments have been performed with mixtures with different composition of the three powders. The mixtures have the same mean particle size, about 488 µm. The bubble behaviour changes significantly due to the differences in particle size distribution. The powders with a wide range of particle sizes show the tendency of segregation and the segregation influences on the bubble behaviour. Gas channels are also observed in some of the experiments.

The study of the effect of particle size distribution on bubble behaviour is an important contribution to verify CFD modelling of fluidized beds. Experimental and computational results are compared, and it is found that multiple particle phases have to be included in the simulations to give a good agreement with the experimental results.

Preface

The Master of Science thesis was carried out at Telemark University College (HiT), Department of Technology, Norway. Telemark University College is one of 26 State Colleges in Norway with more than 4000 full time students and over 400 faculty and staff members. Telemark University College is located in south of Norway. There are five campuses including six departments: Bø, Notodden, Porsgrunn, Skien and Rauland. The thesis title is “Experimental study of bubbling fluidized bed”.

I will firstly thank my supervisor Britt Halvorsen for her great support and guidance, and kind encouragement during the project. I also would like to thank faculty and classmates for their support and help.

There are some notes that readers may pay attention to:

All the references in the text contain the last name of the authors and the year of the publication.

The report is written in Microsoft Word, and then transformed into PDF type with PDFCreator.

The simulations are done by D. G. A. S. U. Ariyarathna with the CFD model at Telemark University College, Norway. The pictures are mostly made in Microsoft Excel, and managed in the Paint.

June, 2008 Wenjun Wu

Contents

1. Introduction

Gas-solid fluidized bed has been applied in industrial process in a wide range. It is usually formed when a quantity of solid particles is forced to behave as a fluid, which is called fluidization. The phenomena mainly happen with the introduction of pressurized fluid or gas, which flows upwards from the bottom of the bed and through the solid medium. Under this situation, the density of the solid medium is reduced without any effects on its elemental nature, and also, the solid particles tend to have many properties and characterizations like a normal fluid, such as the ability to free-flow under gravity, or to be pumped using fluid type technologies. Figure 1.1 shows the model of a typical fluidized bed (http://en.wikipedia.org/wiki/Fluidized_bed).

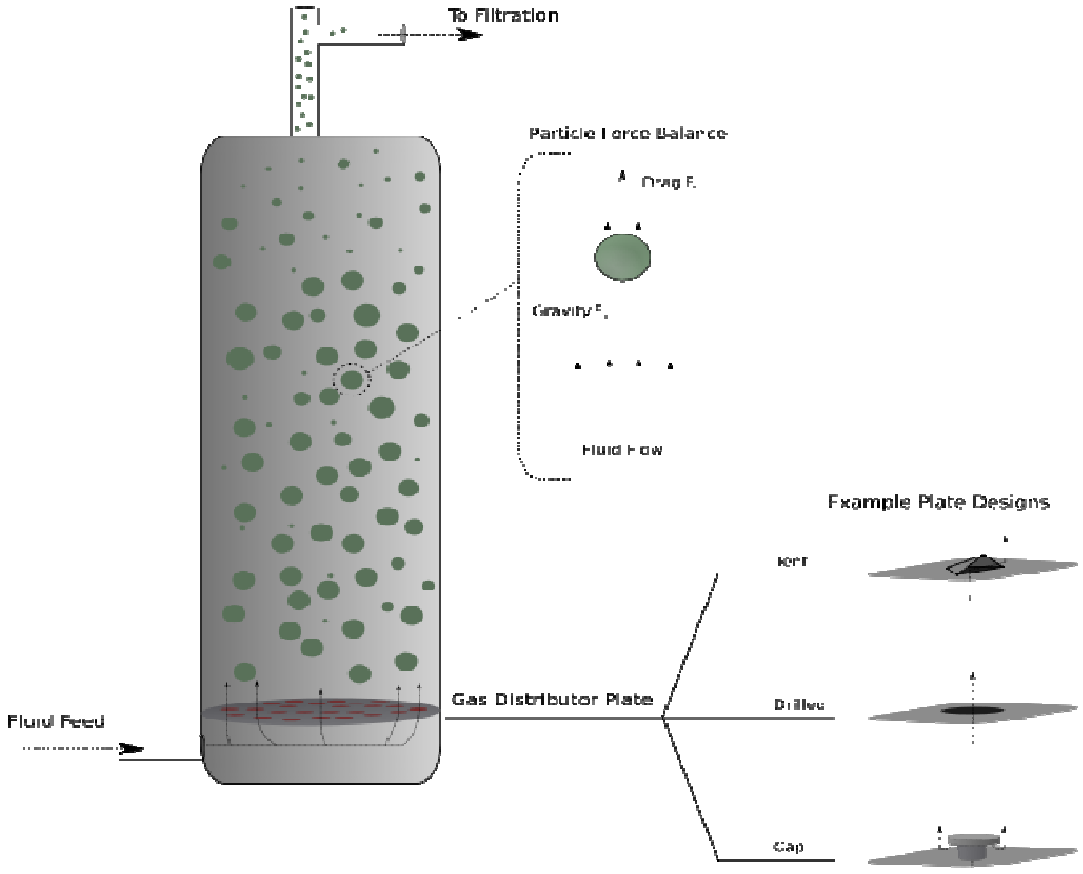

Figure 1.1: A diagram of a fluidized bed, including a particle force balance and distributor plate designs.

The first large scale commercial implementation, in the early 1940s, was the Fluid Catalytic Cracking process, which converted heavier petroleum cuts into gasoline. Carbon-rich "coke" deposits on the catalyst particles and deactivates the catalyst in less than 1 second. The fluidized catalyst particles are shuttled between the fluidized bed reactor and a fluidized bed burner where the coke deposits are burned off, generating heat for the endothermic cracking reaction. In the late 1970s, a fluidized bed process for the

synthesis of polyethylene dramatically reduced the cost of this important polymer, making its use economical in many new applications. The polymerization reaction generates heat and the intense mixing associated with fluidization prevents hot spots where the polyethylene particles would melt. A similar process is used for the synthesis of polypropylene. Currently, most of the processes that are being developed for the industrial production of carbon nanotubes use a fluidized bed as summarized by Baddour and Briens (2005). A new application of fluidization technology is chemical looping combustion. To reduce global warming, it is important to sequestrate the carbon dioxide generated by fuel combustion, e.g. in power stations. Regular combustion with air produces a gas that is mostly nitrogen, which prevents economical sequestration. Chemical looping uses a metal oxide as a solid oxygen carrier. Metal oxide particles react with a solid, liquid or gaseous fuel in a fluidized bed combustor, producing solid metal particles and a mixture of carbon dioxide and water vapor. The water vapor is condensed, leaving pure carbon dioxide which can be sequestrated. The solid metal particles are circulated to another fluidized bed where they react with air, producing heat and regenerating metal oxide particles that are recirculated to the fluidized bed combustor (http://en.wikipedia.org/wiki/Fluidization).

Generally, a gas-solid fluidized bed can behave pretty differently with varied parameters. According to a study by Kunii and Levenspiel (1991), a bubbling fluidized bed can be this kind of fluidized bed: With an increase of gas flow rate beyond minimum fluidization, where a balance is reached between gravity of particles and pressure drop of the flow through any sections of the bed, all the particles keep suspended and still relatively (http://en.wikipedia.org/wiki/Fluidized_bed), large instabilities with bubbling and channeling of gas are observed. When the gas flow rate is increased further, more violent agitation and more vigorous movement of solids show up. Such a bed is called *a bubbling fluidized bed*, or *an aggregative fluidized bed*, or *a heterogeneous fluidized bed*. At this situation, the bed will not expand too much beyond its volume at minimum fluidization.

In Kunii and Levenspiel's study, compared with some other conventional contacting models, the fluidized bed is usually unable to reach the ideal plug flow very closely. Because in a fluidized bed, solids are best presented by well-mixed flow and the gas follows some intermediate and difficult-to-describe flow pattern. Nevertheless, if proper baffling and staging of units and negligible entrainment of solids are available, the desirable extreme of countercurrent of plug flow can still be approached in application of fluidized.

There are some obvious advantages on application of the fluidized bed, for example, it can provide larger contact area among the reactants, further lead to more effective chemical reactions and heat transfer. Therefore the fluidized bed is widely applied for several industrial purposes, such as fluidized bed reactors (types of chemical reactors), fluid catalytic cracking, fluidized bed combustion, fluidized bed bio-filter (used for biological treatment of polluted waters) or applying a coating on solid items (http://en.wikipedia.org/wiki/Fluidization). The fluidized bed has lots of characteristics both desirable and undesirable, based on Kunii and Levenspiel (1991), and Rhodes, M.J (1990), these characteristics can be summarized as the followings:

Advantages:

Easy handled and continuous automatically controlled operation by courtesy of smooth, liquid-like flow of particles; A large margin of safety in avoiding temperature runaway for highly exothermic reactions due to the great resistance on rapid temperature changes in operating conditions, which is given by the large thermal flywheel of well-mixed solids; Good possibility to remove (or add) the vast quantities of heat produced (or needed) in large reactors by reason of well circulation of solids between two beds; High heat (surface to bed, or gas to particle) and mass transfer rates between gas and particles compared to other contacting modes, which is responsible to isothermal conditions radially and axially, due to rapid mixing of solids; Smaller surface area of the heat exchanger required within fluidized bed as a result of high heat transfer rate; Smaller pressure compared to fixed bed with same bubble velocity and bed depth; Good suitability for large-scale operations.

Disadvantages:

Inefficient contacting represented by the difficult-to-describe flow of gas with large deviations from plug flow in bubbling beds of fine particles; Lower reaction rate because a lowering operating temperature is required by the agglomeration, and sintering of fine particles at high temperature for non-catalytic operations; Non-uniform residence of solids led by the rapid mixing of solids. This problem will further develop a non-uniform product and a poorer performance, especially at high conversion levels; The less applicable range of particles because friable solids are easily pulverized and entrained by the gas; Difficult scale-up of the bed due to gas bubbles and further leads to less contact of reacting gas and solids; Erosion of pipes and vessels from abrasion by particles.

Many studies have been done on the gas-solid fluidized bed. The performance of a gas-solid fluidized system is seriously determined by numerous factors, such as the characteristics of the powders, the design of the bed, or the operating conditions. Those previous works focused on many different aspects that may affect the behaviors of the fluidized bed directly or even indirectly, such as size and size distribution of solids, fluid-solid density ratio, vessel geometry, gas inlet arrangement, type of solids used, and whether solids are free-flowing or liable to agglomerate, Kunii D. and Levenspiel O. (1991). Rhodes M.J (1990), Gidaspow D. (1994), Geldart, D., Yeung, S. L. S. (1995), Wong, A. C.-Y., Seville, J. P. K. *et al.*, Ergun, S., Werther, J., Davidson J. F. and Harrison D. and so on have been published and provided lots of references and evidences to support what are written in this present project.

The main objective of this project is to investigate whether and how the bubble distribution, bubble size and bubble velocity can influence the efficiency of fluidized bed reactor. In order to reach this objective, a 2-D fluidized bed was built up with a homogeneous gas inlet, within which different particles with diverse sizes and size distributions and different flow conditions were tested. A camera was used to record the bubble behavior during whole experiments. Besides, some simulations were carried out

in consistent with similar operating conditions of several experiments so as to make a contrast with experimental findings.

2. Literature review

Quantities, which can be recognized as significant factors that determine the fluidization mode and characteristics in a given gas-solid fluidized bed, include the design parameters, superficial fluidizing velocity, minimum fluidization velocity and minimum bubbling velocity, bubble formation, bubble velocity and so on as concluded by M. Horio and A. Nonaka (1987). Those factors are strongly affected by the particles characteristics used in fluidized bed all the time. In the present chapter, the general study and review are given in terms of some previous works.

2.1 Characteristics of the powders

2.1.1 Geldart's classification

In a study from Geldart at 1993, it's been found out that the performance of gas-solid fluidized system is seriously dependent upon the characterization of the particles used as the solid medium, such as density, particle size, fine content, cohesiveness, etc. One statement was widely recognized at early period that a powder with a wide range size distribution fluidized more satisfactorily than a powder having a narrow size range. However, Geldart showed no effect due to size distribution via an experiment on bubble size done at 1972 in sands having a mean particle size. This finding led to the idea of the powder groups, which is commonly called Geldart's classification (1986). According to Geldart classification, the uniformly sized particle can be classified into four groups in terms of the density difference between the particle and the fluid and by the mean particle size for air at ambient conditions, which can be represented on Figure 2.1.

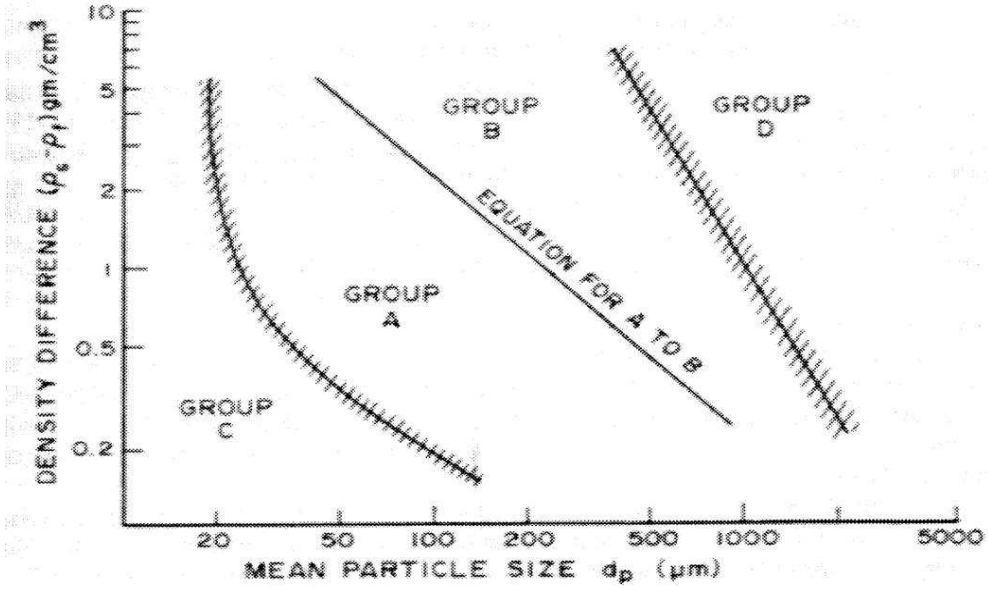

Figure 2.1: Geldart diagram for particle classification.

D. Geldart (1973), M. Rhodes(1990) and D. Gidaspow (1994) have simply summarized the characteristic of each group as the following:

Group C:
All cohesive particles those are hard to fluid. Because the inter particle force is larger than hydrodynamic exerted by fluid gas; Obligated to form channels or cracks through which it passes, rather than forming bubbles; One way to identify is: if HR>1.4, it is considered to be group C particle.

Group A:
Named as aerated particle, into which the materials with a small mean particle size and a low density (<1400 kg/m^3) can be counted. It has most desirable properties for fluidization, and mostly used as catalyst in fluidization system; Considerable bed expansion after minimum fluidization and long time to deaerate after gas supply is interrupted; No bubble produced without higher velocity; Significantly less inter-particle force than hydrodynamic force; Easy to circulate around pneumatic and fluidized circulation loop; Limited size on gas bubbles, which are easily broken down at a high gas velocity.

Group B:
Named by bubbling, the approximate range of mean size of the materials in this group is within 40 to 500 μm, while the density is within 1400 to 4000 kg/m^3; No large expansion of the bed for these materials at atmospheric pressure; The bubbling will start at minimum fluidization.

Group D:
Made of large or very dense particles, can be spout out easily; In this group, gas rises more quickly than gas bubbles, which consequently leads to a phenomena that gas enters the bottom of bubbles, and leaves out through the roof, giving a shorter resistant time; In this group, there will be a transition from bubbling into dispersion regime when the Re>~1000.

The further details about the group properties are shown in Appendix A.

2.1.2 Particle size distribution and particle density

Behaviors of solid particles are largely dependent on a combination of mean particle size and density (Geldart, 1973), usually referred to Geldart diagram for air at ambient conditions.

Particle size distribution

In many practical cases, the working particles usually consist of a few kinds of particles with different sizes. As mentioned above, the particle distribution is also an important factor of determining the bubble behaviors. For convenient rank, the mean particle size can be used to roughly define which group the particle belongs to.

Based on the Geldart diagram, the mean size of particles can be represented as:

$$\bar{d}_P = 1/\sum \frac{x_i}{d_i} \qquad \text{(Eq. 2.1)}$$

where, d_i is Arithmetic mean of adjacent sieves;

x_i is mass fraction.

In most industrial applications, sizing of the particle is usually done by using sieving, which is also used in present study and going to be introduced later on.

Particle density

The ρ_P is defined as the mass of particles divided by its volume, including all the open and closed pores. For "non-porous" solids, gas pyknometer and specific gravity bottle can be used for density measurement. These devices will give a true or absolute density, ρ_{ABS}. This is inappropriate for "porous" solids because ρ_{ABS} includes fluid flow.

The ρ_P is not easy to measure. As represented by Geldart (1990), if the particle is open-pore porosity, and x is known, the ρ_P can be simply obtained from ρ_{ABS}:

$$\rho_P = \frac{1}{1/\rho_{ABS} + x} \qquad \text{(Eq. 2.2)}$$

2.2 Characteristics of fluidized bed

2.2.1 Mechanisms of the fluidization

The fluidized bed will start expanding when the gas flow is great enough to move the solid particles apart. At a certain high velocity of gas flow, a balance will be reached between gravity of particles and pressure drop of the flow through any sections of the bed, all the particles keep suspended and still relatively. This situation is called minimum fluidization. If the velocity of the input air keeps increasing over the minimum fluidization velocity, the instabilities will increase with bubbling, vigorous movement of the solid particles and small expansion of the bed, a bubbling fluidized bed is formed (http://en.wikipedia.org/wiki/Fluidization).

2.2.2 Minimum fluidization velocity

Minimum fluidization velocity is the superficial gas velocity at minimum fluidization conditions, it is an important index of the properties of particles. As described by D. Gidaspow (1993), this velocity could be determined empirically by intersection of the pressure drop versus the superficial velocity curve equals the weight of the bed line. This can be illustrated in Figure 2.2.

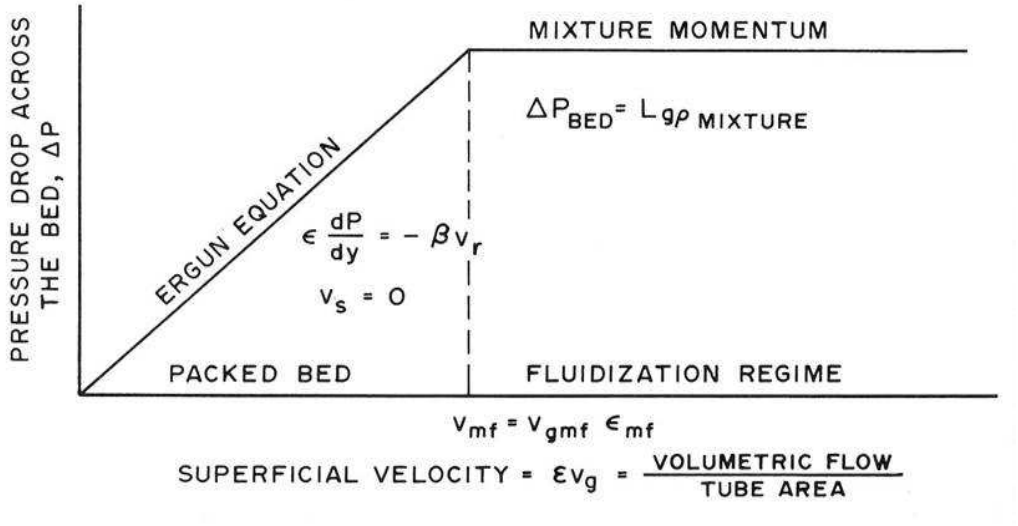

Figure 2.2: Determination of minimum fluidization velocity, D. Gidaspow (1993)

Besides, according to Kunii D. and Levenspiel O. (1991), for a bed of particles resting on a uniform distributor, the onset of fluidization occurs when

$$\begin{pmatrix}\text{drag force by}\\ \text{upward moving gas}\end{pmatrix}=\begin{pmatrix}\text{weight of}\\ \text{particles}\end{pmatrix} \qquad \text{(Eq. 2.3)}$$

Eq. 2.3 can be further rearranged to find out the minimum fluidization conditions that

$$\frac{\Delta p_b}{L_{mf}}=\left(1-\varepsilon_{mf}\right)\left(\rho_s-\rho_g\right)\frac{g}{g_c} \qquad \text{(Eq. 2.4)}$$

The frictional pressure drop through fixed bed of length L containing a single size of isotropic solids of screen size d_p has been correlated by Ergun (1952) by the following equation

$$\frac{\Delta p_{fr}}{L_m}g_c=150\frac{\left(1-\varepsilon_m\right)^2}{\varepsilon_m^3}\frac{\mu u_o}{\left(\phi_s d_p\right)^2}+1.75\frac{1-\varepsilon_m}{\varepsilon_m^3}\frac{\rho_g u_o^2}{\phi_s d_p} \qquad \text{(Eq. 2.5)}$$

By combining Eq. 2.4 and 2.5, a general quadratic of minimum fluidization velocity u_{mf} is given for isotropic-shaped solids

$$\frac{1.75}{\varepsilon_{mf}^3\phi_s}\left(\frac{d_P u_{mf}\rho_g}{\mu}\right)^2+\frac{150(1-\varepsilon_{mf})}{\varepsilon_{mf}^3\phi_s^2}\left(\frac{d_P u_{mf}\rho_g}{\mu}\right)=\frac{d_P^3\rho_g(\rho_s-\rho_g)g}{\mu^2} \qquad \text{(Eq. 2.6)}$$

In special case of very small particles, Eq. 2.6 simplifies to

$$u_{mf} = \varepsilon_{mf} v_{gmf} = \frac{{d_P}^2 \Delta\rho g}{150\mu} \cdot \frac{{\phi_s}^2 {\varepsilon_{mf}}^3}{1-\varepsilon_{mf}}, \qquad \mathrm{Re}_{mf} = \frac{d_P u_{mf} \rho_f}{\mu} < 20 \qquad \text{(Eq. 2.7)}$$

Wen and Yu (1966) have found an approximate relation

$$\frac{1-\varepsilon_{mf}}{{\phi_s}^2 {\varepsilon_{mf}}^3} = A \cong 11 \qquad \text{(Eq. 2.8)}$$

Combine all the above equations, a commonly used estimation for u_{mf} of very small particles can be developed:

$$u_{mf} = \frac{{d_P}^2 (\rho_s - \rho_f) g}{1650\mu}, \ \mathrm{Re}_{mf} < 20 \qquad \text{(Eq. 2.9)}$$

For very large particles,

$$u_{mf}^2 = \varepsilon_{mf} v_{gmf} = \frac{d_P (\rho_s - \rho_f) g}{24.5\rho_f}, \ \mathrm{Re}_{mf} > 1000 \qquad \text{(Eq. 2.10)}$$

The method mentioned above could be applied to estimate the u_{mf} of very small or large particles, but for the particles falling in between, since the Reynolds numbers is beyond the limitation, Eq. 2.6 is more applicable here.

2.2.3 Pressure drop and bed expansion

Pressure drop

As described by Rhodes M.J. (1990), the pressure drop across the powder keeps constant and can be represented with submerged weight of the bed divided by the cross-sectional area of the column.

$$\Delta p = (\rho_p - \rho_g)(1-\varepsilon_{mf}) H_{mf} g \approx \rho_{BS} H_S g \qquad \text{(Eq. 2.11)}$$

where ρ_{BS} is the bulk density of the gently settled bed;

H_S is the height of the gently settled bed.

Since ρ_g is much less than ρ_p, then

$$\Delta p = \frac{M_B g}{A} \qquad \text{(Eq. 2.12)}$$

where $M_B g$ is the submerged weight of the bed;

A is the cross-sectional area of the column.

Bed expansion

Bed expansion can also be explained as a decrease of bed density with an increase of gas flow rate. This phenomenon is mostly caused by the hold-up of the gas bubbles, which the characteristics are governed by the amount of the gas appearing as "visible" or discrete bubbles, and the speed at which they rise. The "visible" volumetric flow rate of bubbles can be expressed as:

$$Q_B = Y(U - U_{mf})A \qquad \text{(Eq. 2.13)}$$

where 0.8<Y<1, for group A powders;

0.6<Y<0.8, for group B powders;

0.25<Y<0.6, for group D powders.

The expansion can be expressed in terms of the fraction of the bed occupied by bubbles:

$$\varepsilon_B = \frac{H - H_{mf}}{H} = \frac{Q_B}{A\bar{U}_B} = \frac{Y(U - U_{mf})}{\bar{U}_B} \qquad \text{(Eq. 2.14)}$$

where, H is the average height of the bed at velocity U;

H_{mf} is bed height at velocity U_{mf};

$\bar{U}_B$ is the average velocity of bubbles, usually calculated using bubble size at middle height of bed.

2.3 Characteristics of bubble size

Bubble size is one important factor that strongly affects behaviors of a fluidized bed of particles, and also has a lot to do with others properties of a fluidized bed. As indicated by Kunii D. and Levenspiel O. (1991), basically, the limiting bubble size is smaller in fine particle system than in large particle system.

For Geldart B solids, there are several correlations have been developed to estimate the bubble growth in fluidized beds from experiments mainly in small-diameter beds but as well as for large-diameter beds due to GOLFERS (1982).

For a bed of Geldart B solids supported by a porous plate distributor, Werther (1981) has given an approach to calculate the bubble size at any height z, as expressed below:

$$d_b = 0.853\left[1 + 0.272(u_o - u_{mf})\right]^{1/3}(1 + 0.0684z)^{1.21} \qquad \text{(Eq. 2.15)}$$

With an applicable range of operating conditions:

d_t <20 cm $\quad 1 \le u_{mf} \le 8$

$100 \le d_p$ <350 μm $\quad 5 \le u_o - u_{mf} \le 30$ cm/s

This expression shows that the bubble diameter at any height z is dependent on the distance z above, and on the amount by which the gas velocity exceeds the minimum fluidization velocity (u_o-u_{mf}). Since the limitations on operating conditions, this equation will be used just roughly to make a comparison with experimental results later.

2.4 Characteristics of bubble velocity

The situation of the gas passing through the bed strongly determines the bed behaviors. Bubbles are the form in which most of the gas passes through the bed, and they determine the gas residence time in the bed, it is necessary to say something on this parameter.

Many approaches have been announced by researchers as Darton *et al.*, Morooka *et al.*, Werther. Based on analyzing the experimental data, Werther (1986) reported the following correlations which fit the experimental data well:

$$u_b = 1.6\left\{\left(u_o - u_{mf}\right) + 1.13 d_b^{0.5}\right\} d_t^{1.35} + u_{br} \qquad \text{(Eq. 2.16)}$$

This expression is applicable for Geldart B solids with the diameter of the bed $d_t \leqq 1$ m. The rise velocity of single bubbles, u_{br}, is proposed by Davidson and Harrison (1963):

$$u_{br} = 0.711(g d_b)^{1/2}, \qquad \frac{d_b}{d_t} < 0.125 \qquad \text{(Eq. 2.17)}$$

2.5 Other relevant properties

Except for those properties introduced above, there are also some other properties which might not be so related to but still have the influence on the behaviors of the fluidized bed. Here some relatively relevant properties with the behaviors of fluidized bed will be introduced.

AOR and bulk density

AOR and bulk densities are two significant parameters required here for estimating the minimum bubbling velocity (u_{mb}) and minimum fluidization velocity (u_{mf}) to predict the fluidization behavior of a powder. AOR is the abbreviation of “angle of repose” which is a physical property of the powders; there are two types of bulk density, aerated and tapped bulk density (ρ_A and ρ_T). the bulk density can be measured by the “caking end-point” method demonstrated by Yeung (1995) and Wong (2000).

There are two reasons to select these parameters: firstly the methods for determination of these two parameters are simple, inexpensive, re-producible and no requires of the tedious experiments; secondly, these two parameters are measured when "flow", therefore they can reflect the flowability and dynamic fluidization behaviors of a powder better.

Here one new term needs to be introduced, the "weighted" AOR, which is equal to AOR/$\rho_{A,}$or modified "weighted" AOR, which is AOR/ρ_T. This property has a strong relationship with u_{mb} and u_{mf}. This can be shown in the diagram below according to Anthony Chi-Ying Wong (2002).

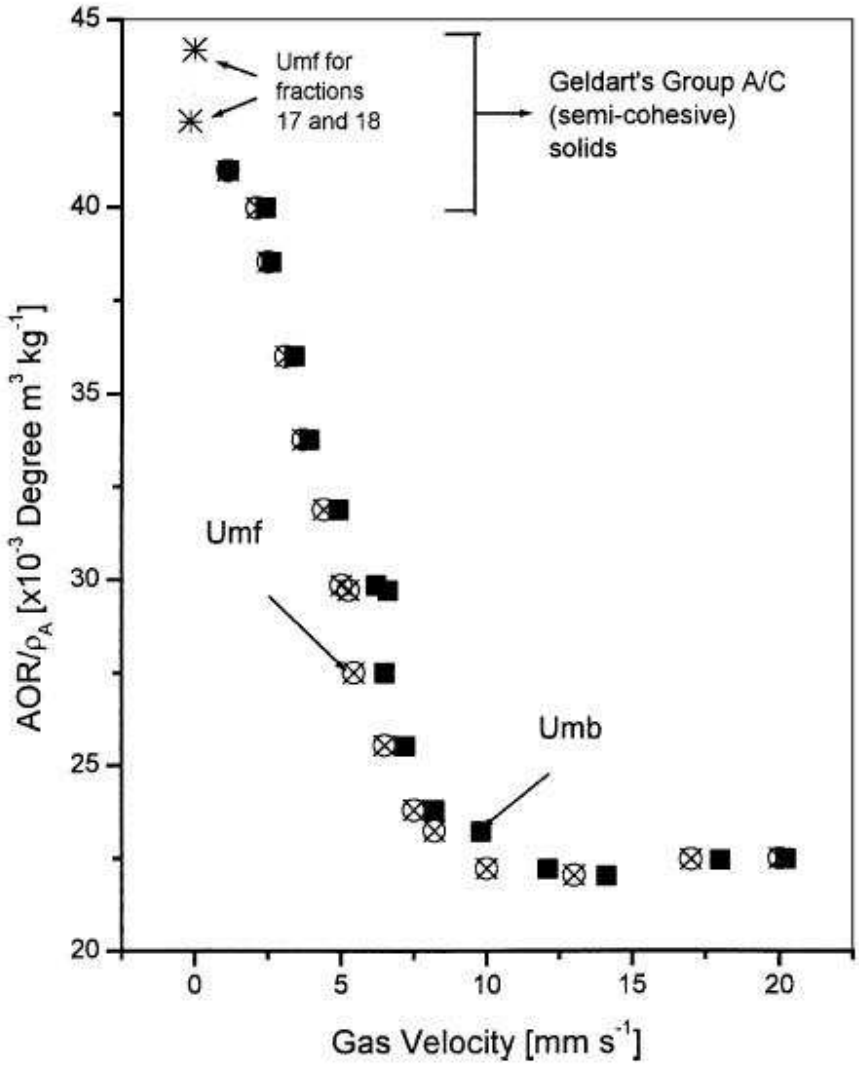

Figure 2.3: Diagram showing "weighted" AOR as function of u_{mf} and u_{mb}, by Anthony Chi-Ying Wong (2002).

HR

The Hausner ratio, which is referred as the ratio of ρ_T to ρ_A, is a reasonable indicator as well as AOR for a powder's characteristics (Wong, 2000). Increase of HR represents a bigger difference between ρ_T and ρ_A; when HR>1.4, the powder behaves more likely a cohesive powder. The relationship between "weighted" AOR and HR is presented in Figure 2.4. In an early study by Wong (2000), AOR and HR showed a rather sharp increase when d_P was less than ~100 µm. this finding also confirmed a general understanding that the larger the AOR and HR, the more cohesive the powder-due to the increasing inter-particle force as the particle size decreases due to Seville, Willett and Knight (2000).

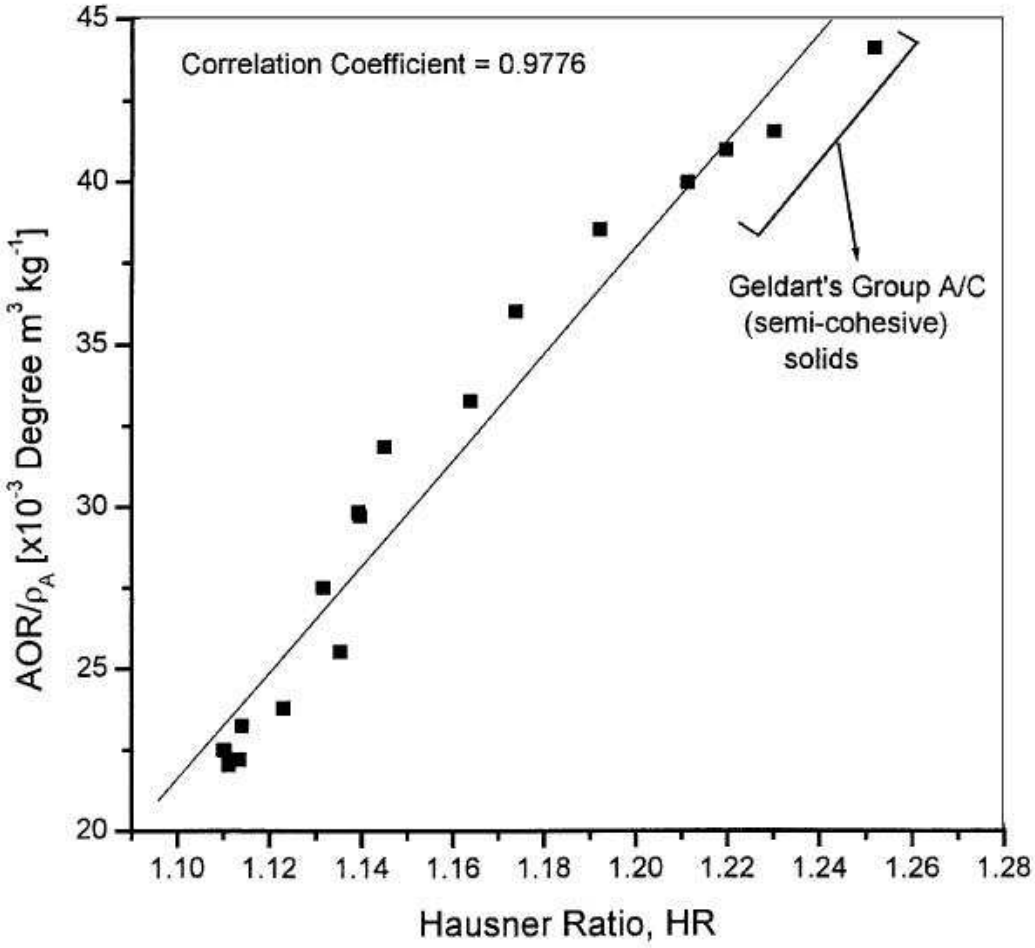

Figure 2.4: Relationship between "weighted" AOR and HR, by Anthony Chi-Ying Wong (2002).

According to Wong (2002), both the ratio of AOR to bulk density (or modified "weighted" AOR) and HR exhibited a strong exponential decaying characteristics with either u_{mb} or u_{mf} as Eq. 2.18:

$$y = A + Be^{-x/C} \qquad \text{(Eq. 2.18)}$$

where A= y offset;

B= amplitude;

C= decay constant.

These values were summarized in Table 2.1.

Values of constant (Eq. (1)) and correlation coefficient of different plots

Plot	Constants (Referring to Eq. (1))		Correlation Coefficient
$\frac{AOR}{\rho_A}$ vs. U_{mf}	A	20.03	
	B	25.56	0.9467
	C	5.20	
$\frac{AOR}{\rho_T}$ vs. U_{mf}	A	18.07	
	B	18.60	0.9305
	C	5.84	
$\frac{AOR}{HR}$ vs. U_{mf}	A	25.17	
	B	22.53	0.8866
	C	7.25	
$\frac{AOR}{\rho_A}$ vs. U_{mb}	A	20.66	
	B	28.51	0.9564
	C	4.91	
$\frac{AOR}{\rho_T}$ vs. U_{mb}	A	18.59	
	B	20.90	0.9453
	C	5.39	
$\frac{AOR}{HR}$ vs. U_{mb}	A	25.90	
	B	25.27	0.9089
	C	6.54	

Table 2.1: Values of constant (Eq. 2.18) and correlation coefficient of different plots, by Anthony Chi-Ying Wong (2002)

There is a sharp finding that it is better to use the "weighted" AOR rather than the modified "weighted" AOR to correlate with u_{mb} or u_{mf}.

3. A review of measurement methods

To obtain accurate results from experiments, it is very important to select a suitable measurement method in terms of the purpose of one certain study. This chapter will give a general idea on some advanced techniques those are particularly intended for academic investigations of basic fluidization phenomena within lab-scale or still under development. Examples include sensor techniques, imaging and photographic methods. A general summary made by J. Werther (1999) together with some other relevant researches provide lots of resources on this subject.

3.1 Probe Techniques

Due to some obvious merits, eg., simple design, high signal-to-noise ratios, low disturbance, fiber optical probes are quite popular in fluidization research. An extensive overview has been give by M. Louge (1996) on this technique. One example can be hold to show the basic principle of the probe used in Rensner and Werther (1993). As shown in Figure 3.1, the main principle is to use the light emitted by a laser diode to measure volume. This light is produced and then guided by the optical-fiber from the diode to a fiber-optical beam splitter, then to the sensor fiber. This same light is scattered at particles, and then received and transformed back via the same fiber to the photo diode to produce images.

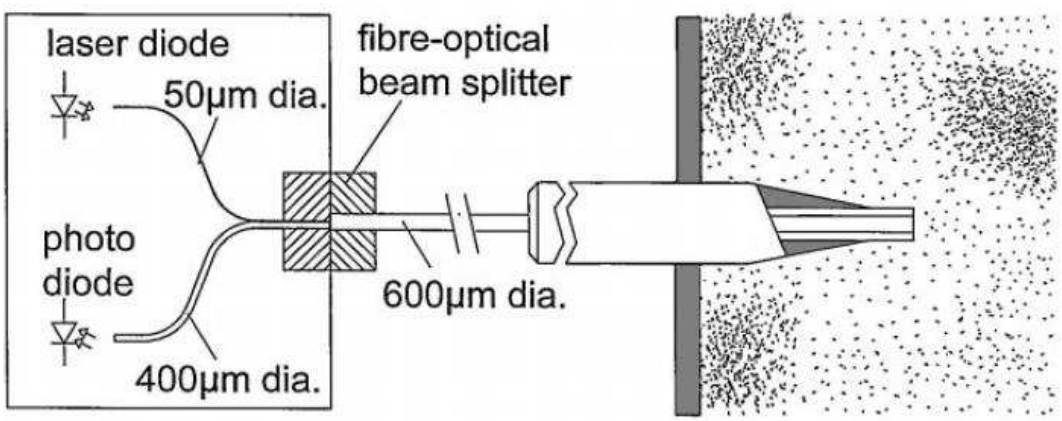

Figure 3.1: Measuring principle of a single-fiber optical probe, D. Rensner et al. (1993).

There still are some difficulties in the practical application of probe techniques. One is, for the measurement of solids volume concentrations in the fluidized bed, optical probes have to be calibrated due to a fact that it is pretty hard to distinguish homogeneous gas-solid suspensions over a wide range of solids concentrations. Some solutions have been provided against this problem. Hartge et al. (1988) developed the shape of the calibration curve by immersing the probe into water-fluidized beds and fixed it by dipping it into a gas-solids system. This calibration is argued by Lischer and Louge (1992) with another

calibration via a comparison with a capacitance probe. More details about solutions are provided by E. U. Hartge et al. (1986), Y. Tung et al. (1988) and W. Zhang et al. (1991).

Another difficulty with the optical fiber probe is limited extent of the measurement volume interrelated to the penetration of light into the suspension. Attempts are made to supply solutions on this problem. A converging arrangement of separate emission and detection fibers are used by Reh and Li (1991) to partly avoid this concentration-dependent variation of measurement volume. Tanner (1994) used a small lens to approach the limitation in order to optimize the measurement volume. This principle, as shown in Figure 3.2, is the basis of measurement system which is presently applied in process industries according to MSE Meili (1996).

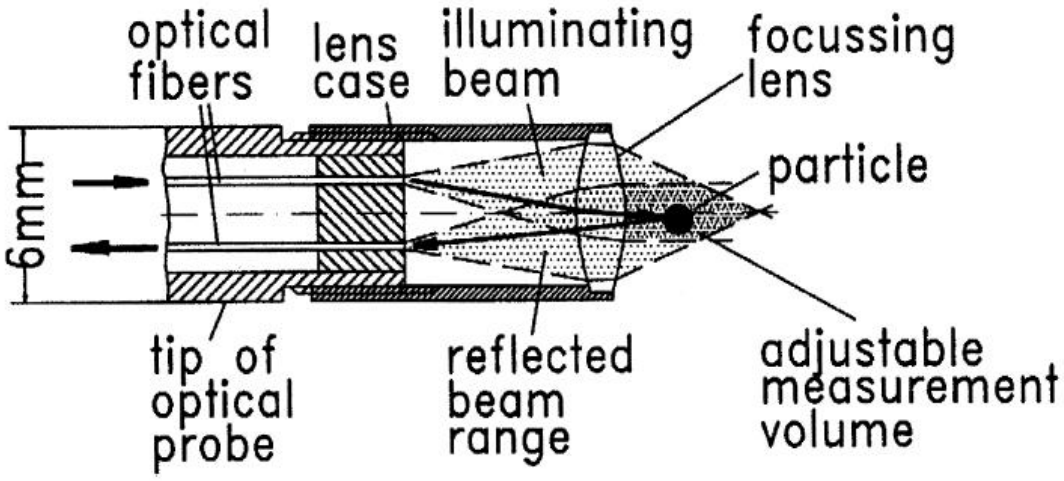

Figure 3.2: Optical probe with limited measurement volume, H. Tanner et al. (1994).

The advent of fiber-optical Laser Doppler Anemometry (LDA) system comes over the problem caused solids volume concentrations which are generally too high to permit a visual observation inside the bed. Figure 3.3 shows such an LDA probe which is firstly used by J. Werther et al. (1996). This probe can be installed inside fluidized bed, the laser light is guided through optical fibers to the former one's head. The measurement volume is established at the cross-point of two laser beams 19 mm in front of the 22 mm diameter probe.

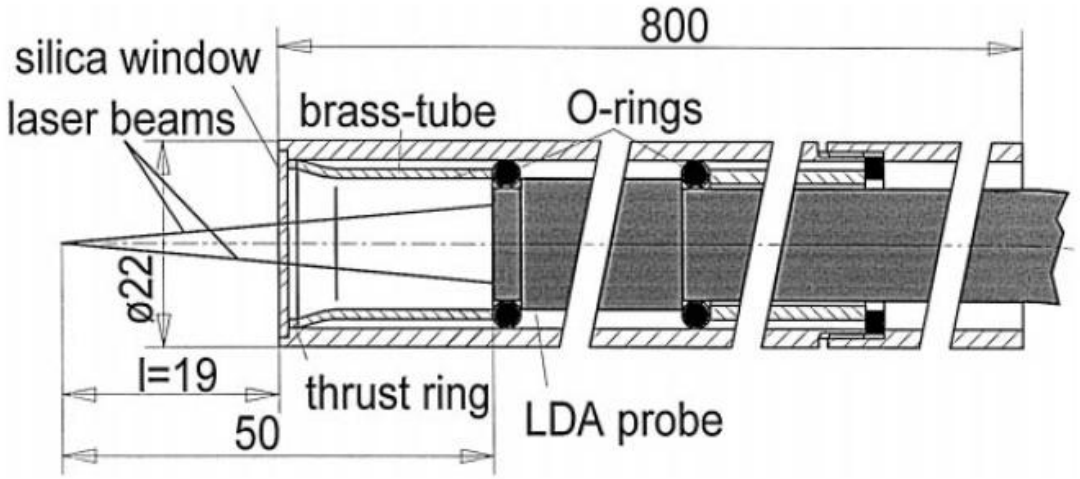

Figure 3.3: LDA probe holder with DANTEC FibreFlow probe (dimensions in mm). J. Werther et al. (1996).

3.2 Non-invasive measurement techniques

Due to the merit that it does not interfere with the flow inside the bed, non-invasive measurement techniques are desirable in wide range. This technique determines properties of the gas-solid flow by means of an instrument located outside the fluidized bed. A big challenge for this technique is big dimensions of reactors in industrial applications. Due to this limitation, applications of this technique are presently restricted into academic investigations of fluidized beds with diameters between 5 and 50 cm in most cases.

Computer Assisted Tomography (CAT)

Recently, tomographic methods are a strong point where significant progress has been made. As demonstrated by Beck et al. (1993), Holoboff et al. (1995), Kantzas and Kalogerakis (1996), the X-ray Computer Assisted Tomography (CAT) is used in their studies on fluidization properties. The CAT scanner is a commercially available instrument for medical use. It permits a resolution of 400 µm by 400 µm in cross-section, the thickness of each imaged slice of the column being 3 mm. The time required for a single scan is 3 s. The processing of the data requires another 40 s.

Capacitance tomography

The capacitance tomography is an alternative option. This technique reconstructs the two-dimensional distribution of the effective dielectric constant from capacitance measurements between pairs of electrodes. It can be schematically represented in Figure 3.4 which is developed by Huang et al. (1989, 1992). The main components include an eight-electrode capacitance sensor, a data collection system and an image reconstruction computer. Eight metal plates are mounted from the sensor on the outer surface of the

insulating pipe section. The capacitance between any two of the eight electrodes is measured by the data collection system. Then the measured values are processed in the computer together with the amplitude of which depends on the dielectric distribution in the tube. This method can reconstruct the cross-sectional image of the component distribution by using a linear back-projection algorithm.

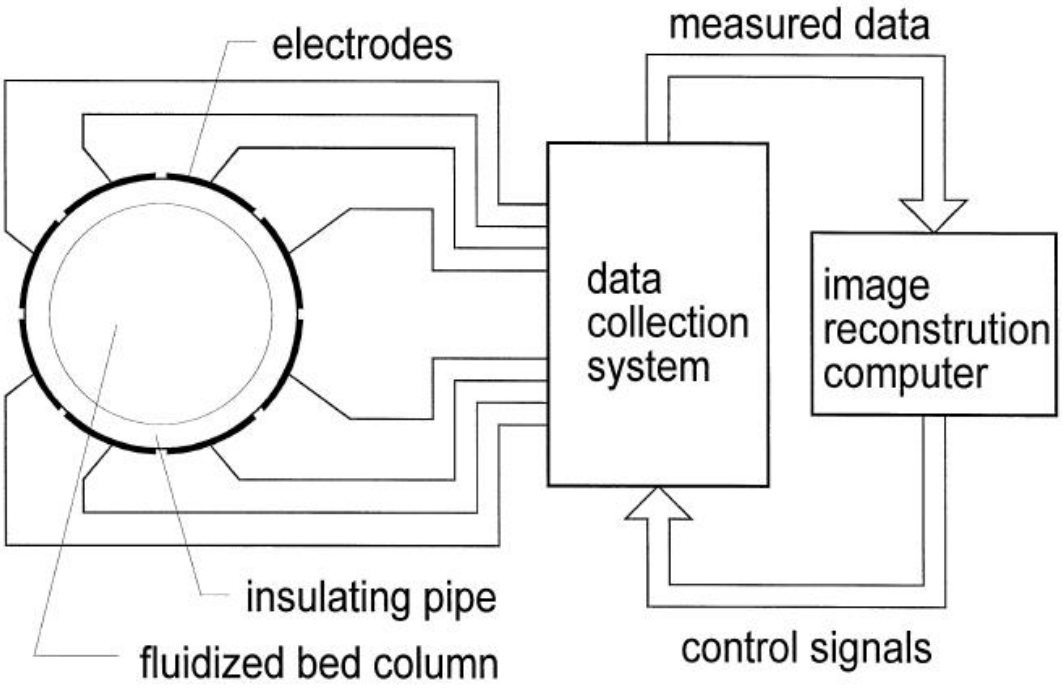

Figure 3.4: Capacitance flow imaging system, Huang et al. (1989).

Figure 3.5 shows a measurement system developed at the US Department of Energy's Morgantown Energy Technology Center (1993). This system involves four rings of 32 electrodes of 25 mm height which are arranged on the circumference of a 150 mm ID cyclindrical fluidized bed. Guard electrodes are intended to minimize the effects of stray capacitance and extend 150 mm above and below the sensor arrangement.

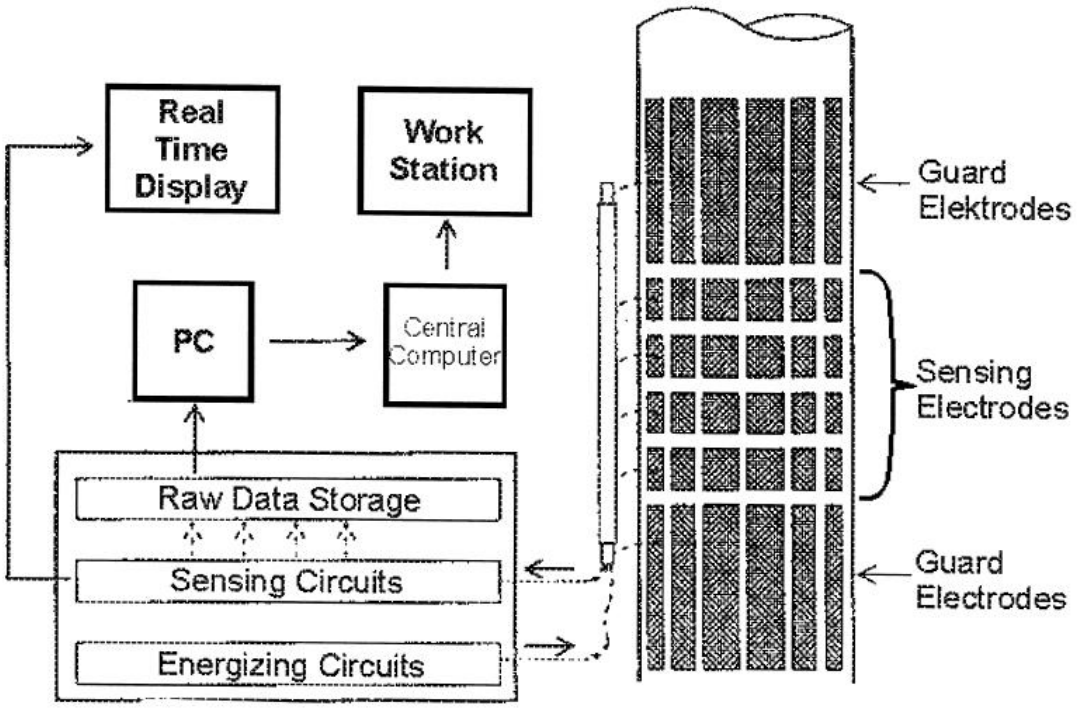

Figure 3.5: Capacitance sensor arrangement used by Halow et al. (1993).

Particle tracking methods

In recent years, particle tracking methods are more commonly applied to investigate some more detailed information on properties of the fluidized bed, eg., solid flow, large-scale circulation patterns and the residence time of a particle. Positron Emission Tomography is typical one used by Seville et al. (1995). The idea of this method is normally applied in the field of medicine. It is basically performed to characterize imaging by means of radiolabelled metabolic fluid. The working principle is constructed on the basis of two collinear γ-ray, which is produced from an annihilation of the initial energy of positrons emitted by a radionuclide. These two collinear are able to be detected in large-area position-sensitive detectors, the line on which the positron emitter lies is therefore determinable.

3.3 Imaging techniques

There are some commonly considered methods used to take images through a fluidized bed. To obtain images with better quality, the particle image velocimetry, proposed by R. C. Chen et al. (1992), Z. Zheng et al. (1992) and S. J. L. Rix (1996), is normally a good choice which is based on a double or multi-exposure photography and functions based on the track of specially marked tracer particles. Zheng et al. (1992), Wirth and Seiter (1991) have performed relevant experiments by using this method. According their results, some

important properties, eg., particle velocity and the residence time of particles, could be determined.

Figure 3.6 shows the set up used by Li et al. (1991). This kind of intrusive optical probes can provide a microscopic view of local phenomena inside the fluidized bed. It is basically constituted by a set of lenses and a fiber-optic flashlight-transmitter.

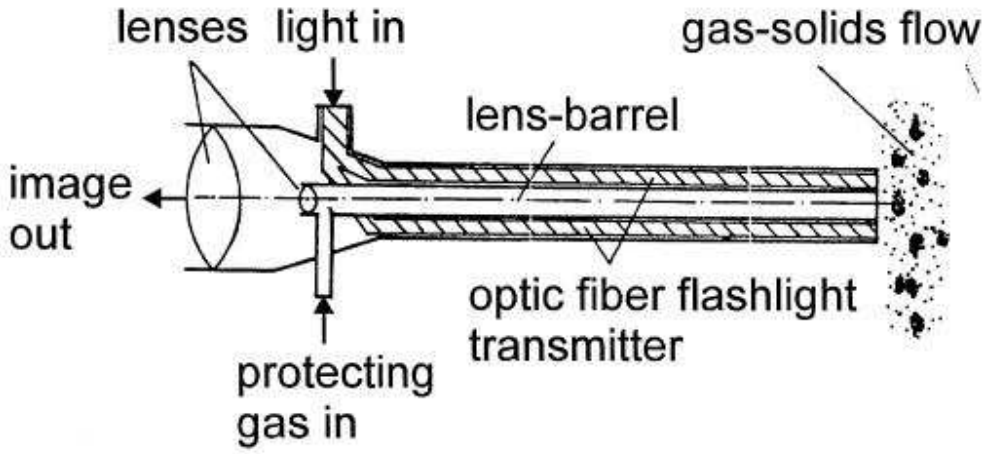

Figure 3.6: Optic fiber micrograph probe, Li et al. (1991).

On the other hand, the X-ray imaging is a powerful tool to obtain a broad view of the fluidized bed. Figure 3.7 illustrates details of this method described by Gamblin et al. (1993). A pulsed beam is produced from a rotating anode, and passes through a shuttering device synchronized with a video camera. The shuttering device allows one X-ray pulse through the fluidized bed each operating period. The produced image on the image intensifier is recorded on the video tape. The motion within the bed is therefore seized, then the instant-in-time representation of the internal structure of the rapidly changing system is given.

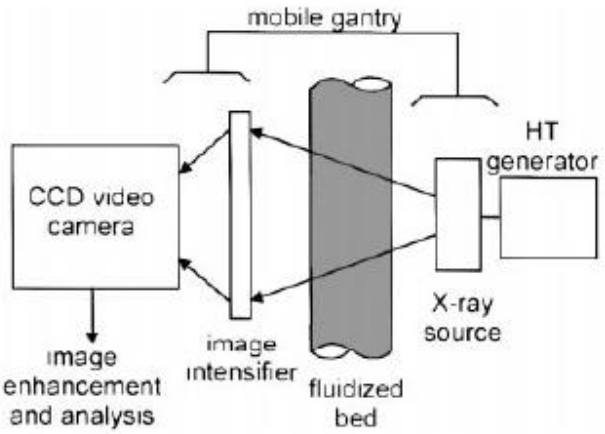

Figure 3.7: X-ray imaging principle, Gamblin et al. (1993).

This method is early pioneered by Rowe et al. (1971) and focused on the phenomena of bubble formation, including bubble velocity, size and shape. However, the main drawback of the X-ray imaging method is that the picture is necessarily silhouetted and hard to distinguish bubbles behind or partly behind others. Therefore, there are always limitations on the thickness and fluidization velocity of the bed.

Recently, attempts on laser sheet light have been made since it can provide a well-defined visualization of flow phenomena inside a fluidized bed. Figure 3.8 illustrates the arrangement used by Horio and Kuroki (1994). Three laser sheets intersecting at right angles need to be applied in addition to see the patterns in vertical and horizontal planes.

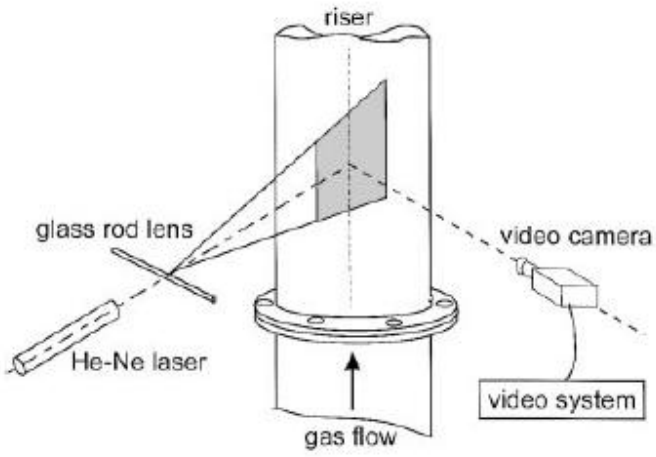

Figure 3.8: Flow visualization by laser sheet, Horio and Kuroki (1994).

Kuroki and Horio (1993) also provide a modified set up in order to come over the main resistance to the penetration of the light due to the presence of the dense wall zone in fluidized bed. As shown in Figure 3.9, a hood with plastic transparent cover is used to guide the laser sheet into the riser. A CCD camera is introduced into the bed with a transparent cover in front.

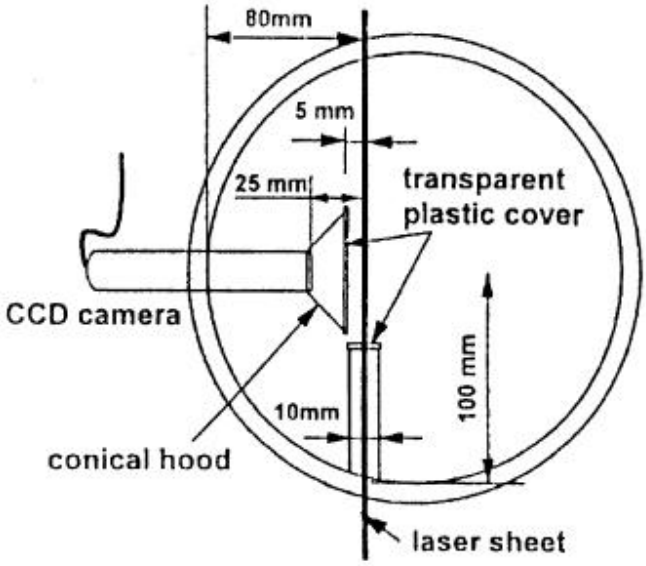

Figure 3.9: ‘Internal imaging’ set-up, Kuroki and Horio (1993).

4. Experimental study

A fluidized bed is purposely designed and built for researching the bubble behavior in two-dimension with a uniform porous air distributor experimentally. The formations and velocities of bubbles with both different flow conditions and particle characteristics are going to be investigated in this study.

4.1 Measurement of particle size distribution

Three groups of particles are measured with range of sizes 100~200 µm (small particle), 400~600 µm (medium particle) and 750~1000 µm (large particle) respectively. The particle size distributions for three powders are measured and listed in Appendix B in detail. In this study, the method "machine sieving" and the device, Retsch AS 200 vibrator, were used together with 5 sieves of different sizes for each group in order to separate particles with different diameters. The diagrams below show the results:

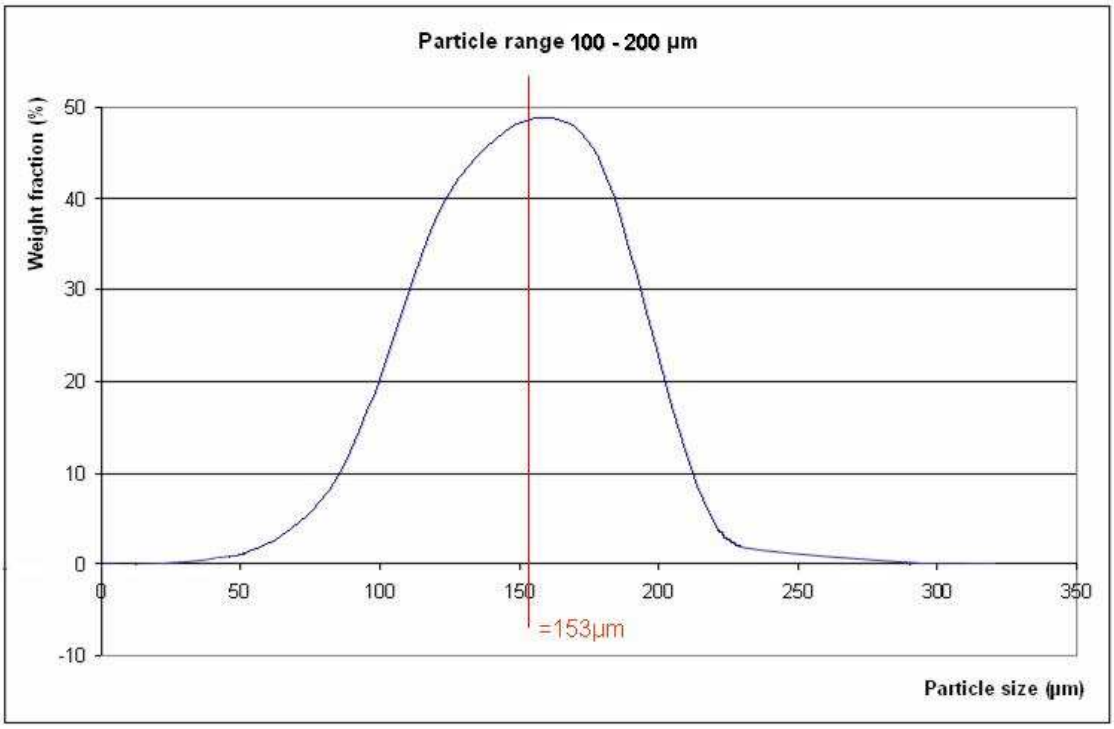

Figure 4.1: Particle size distribution for small particles (100~200 µm).

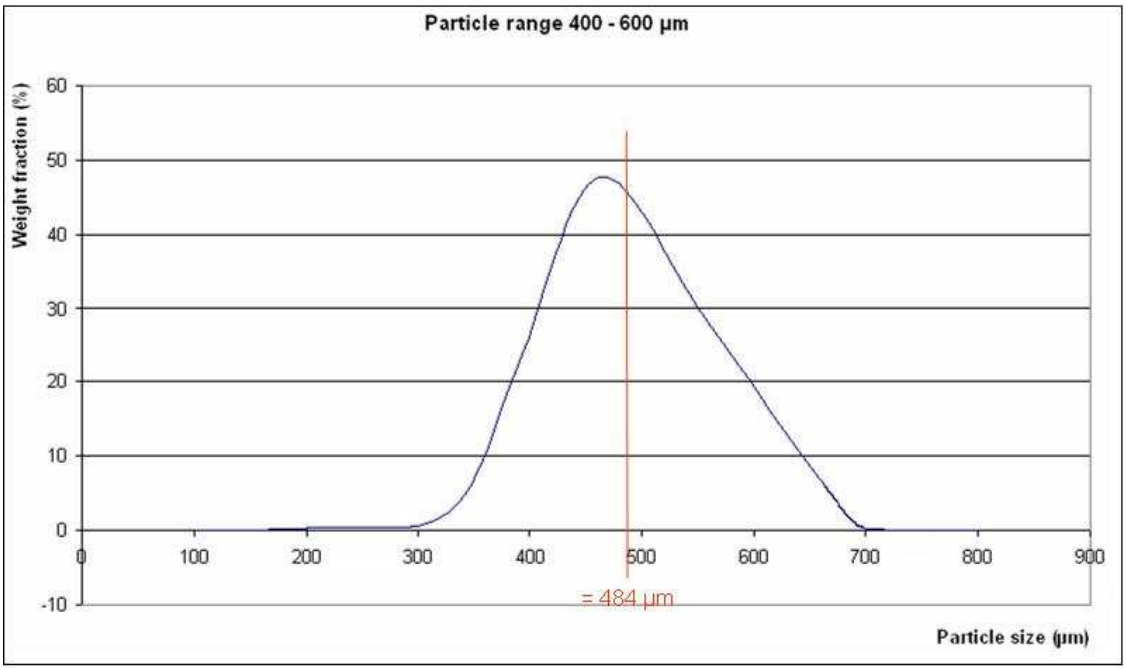

Figure 4.2: Particle size distribution for medium particles (400~600 µm).

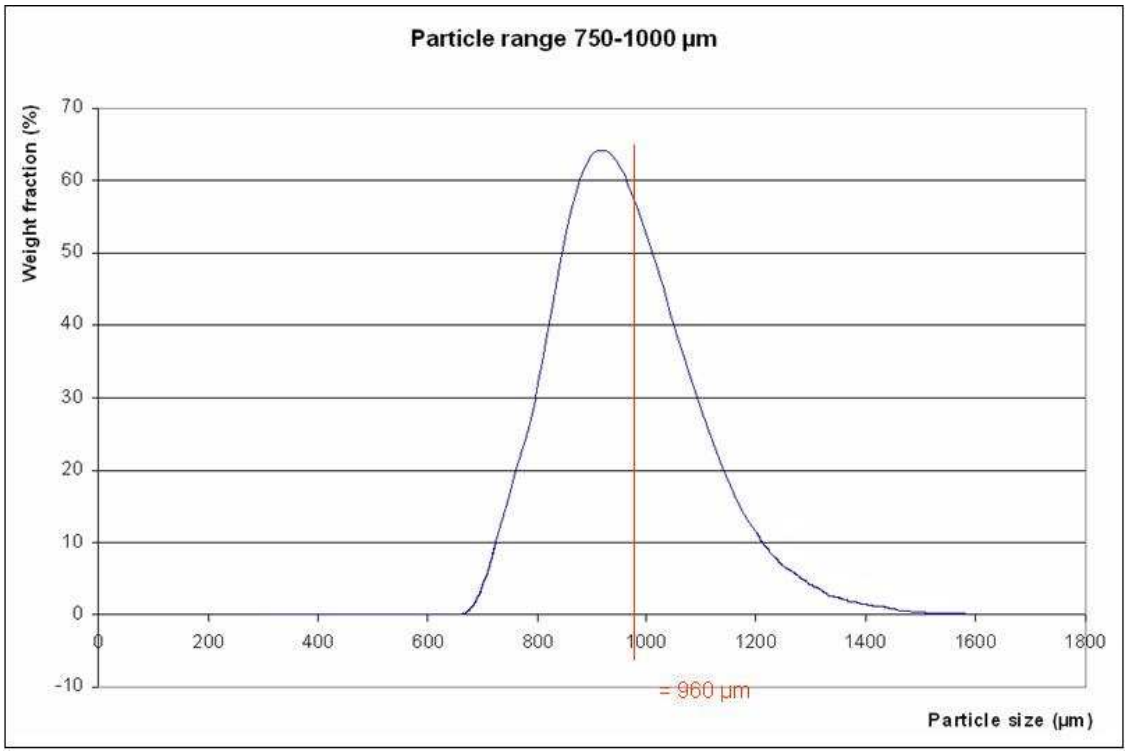

Figure 4.3: Particle size distribution for large particles (750~1000 µm).

In this study, the Arithmetic mean (Rhodes M.J.) is introduced here. It is difficult to verify exactly which sizes are dominant in each groups, the mean values are therefore calculated here to roughly represent the groups. Consequently the mean particle size could be figured out for each group of particles according to Figure 4.1~4.3:

Range of particles (µm)	100~200	400~600	750~1000
Mean particle size (µm)	153	484	960

Table 4.1: Mean particle sizes for each range of particles used in experiments.

According to Geldart's classification (1986), for particles with density 2485 kg/m^3, the Geldart group B ranges from around 120 to 930 µm. according to this, the whole range of particle size for the medium particle is within Geldart group B, parts of the particle size for small and large particle are over group B.

Indeed, most instruments and methods of particle size analysis give the cumulative distribution directly due to its convenience to plot. Figure 4.4, 4.5, and 4.6 show the cumulative distribution for powders with size ranges 100~200 µm, 400~600 µm and 750~1000 µm respectively below:

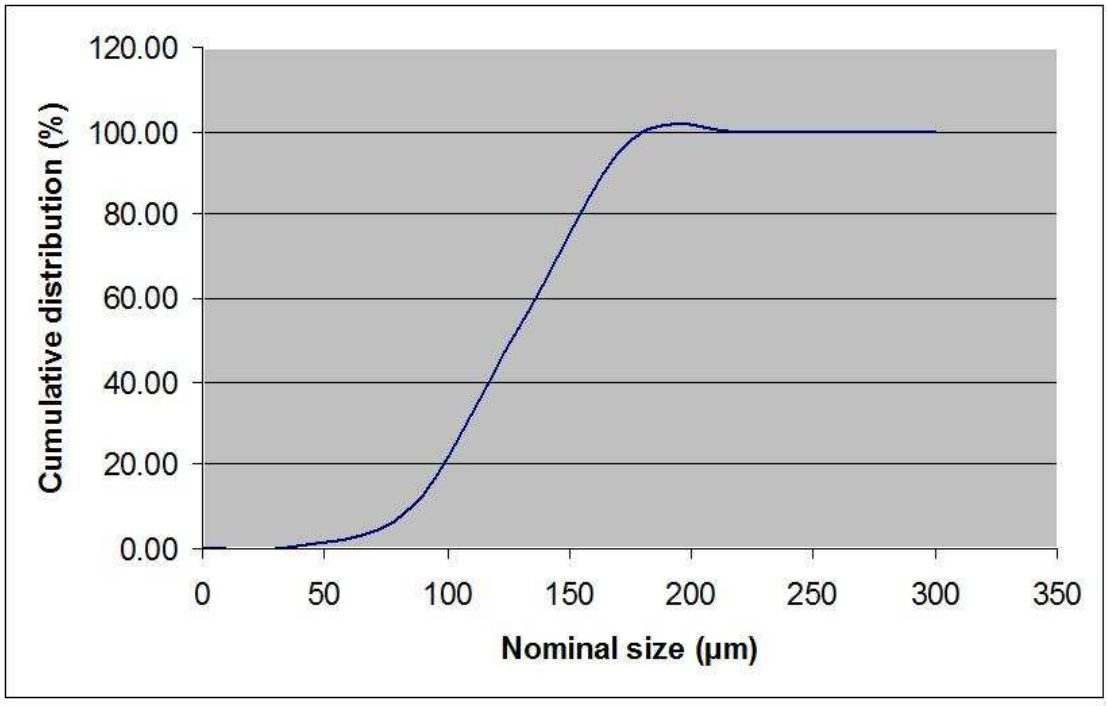

Figure 4.4: Cumulative particle size distribution for small particles

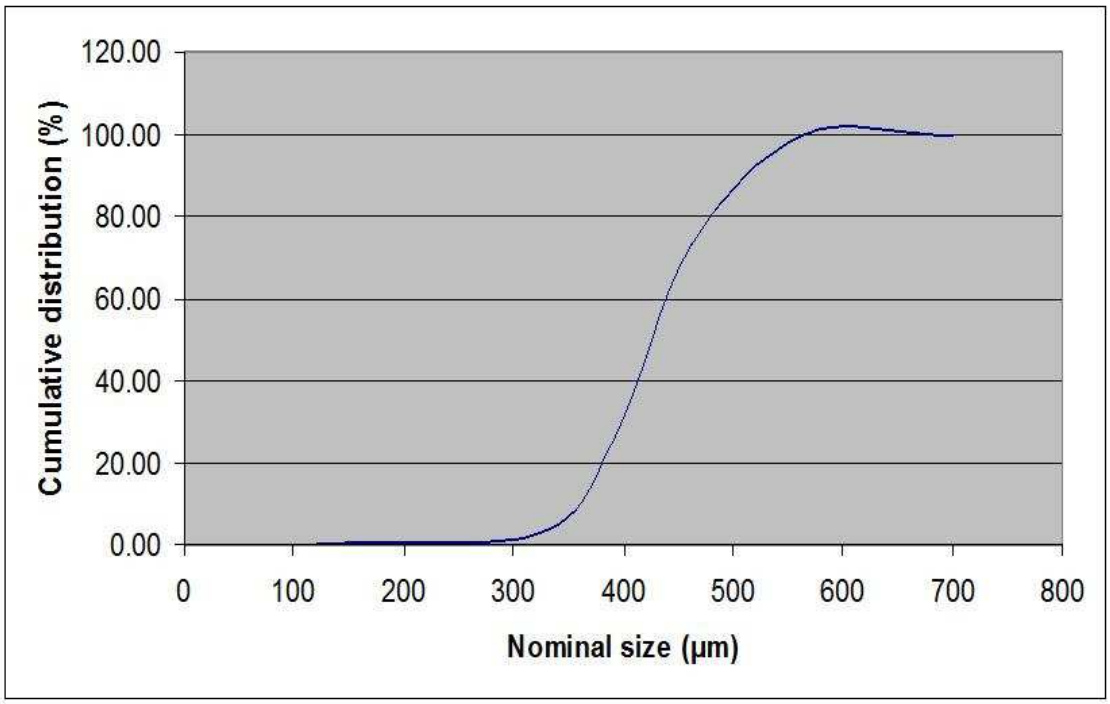

Figure 4.5: Cumulative particle size distribution for medium particles

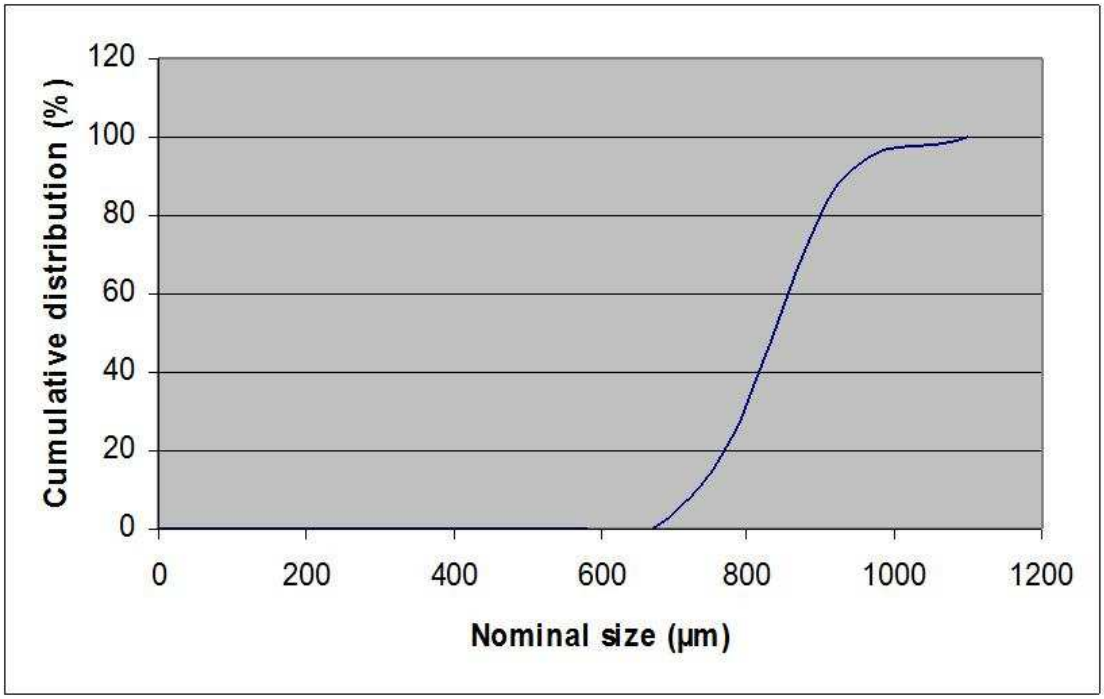

Figure 4.6: Cumulative particle size distribution for large particles

4.2 Experimental set-up

The fluidized bed is made of Lexan glass plate, with dimensions of 0.8 m (height) × 0.2 m (width) × 0.025 m (depth), which can be considered as a two-dimensional reactor. The whole experimental set-up is shown in Figure 4.7.

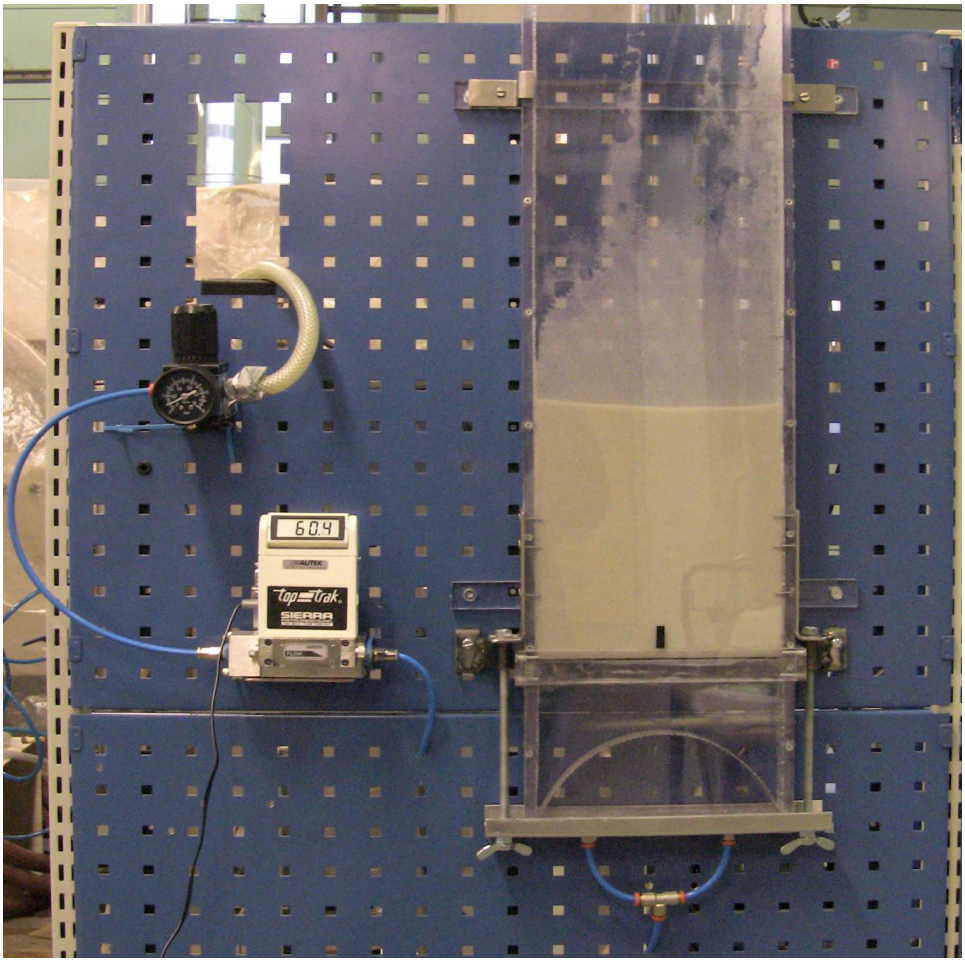

Figure 4.7: Experimental set-up

Glass particles with three different mean particle sizes are used here. Those particles have the sizes ranged from 100~200 µm (small particle), 400~600 µm (medium particle) to 750~1000 µm (large particle) respectively, with similar particle densities approximately equal to 2485 kg/m^3. The structure of the fluidized bed is transparent, behaviors inside the bed could be therefore recorded without any back-lights by a video camera (Canon DC50). The digital visual acquisitions are obtained at a frequency of 30 Hz. A gas valve is applied here to control the gas flow, and a flow-meter is used to show the gas flow rate.

Eq. 2.9 and 2.10 introduced in chapter 2 can be applied to estimate the minimum fluidization velocities for each group of particles. By checking the Reynolds numbers, u_{mf}

for small and medium particles, which are 0.0192 and 0.192 m/s respectively, are confirmed to be reasonable because the Reynolds numbers are within the required region**.** But for the large particle, the value produced from Eq. 2.10 can not be used since the Reynolds numbers is out of the required region. Hence, the general Eq. 2.6 needs to be applied for this powder.

Here, all the glass particles applied in this experiment could be roughly recognized as spherical shape, according to D. Gidaspow (1994):

μ=0.000018 pa$\cdot$s, ϕ=1

The volume fraction at minimum fluidization conditions, ε_{mf}, can be determined by a given equation summarized in D. Gidaspow's study (1994):

$$\varepsilon_{mf} = 1 - \frac{V_p}{V_{m,bulk}} = 1 - \frac{m_p / \rho_p}{m_p / \rho_{m,bulk}} = 1 - \frac{\rho_{m,bulk}}{\rho_p} \qquad \text{(Eq. 4.1)}$$

Here, $V_{m,\ bulk}$ and $\rho_{m,\ bulk}$ are the volume and density of particles within the bed respectively at minimum fluidization. $V_{m,\ bulk}$ can be recognized as a combination of V_{bulk} and bed expansion due to the fluidization. V_{bulk} and ρ_{bulk} are measured by weighting a certain volume of particles. The results are also included in tables below.

Design			
Height	80 cm	Width	20 cm
Depth	2.5 cm	Distributor area	20 × 2.5 cm
Particles (Spherical glass)			
100~200 µm (small)			
Mean particle size (µm)	152	Solid density (kg/m^3)	2485
Air velocity (m/s)	0.13~0.21	Bulk density (kg/m^3)	1530
u_{mf} (m/s, theoretical)	0.019	Bed height (cm)	28, 35
ε_{mf}	0.416, 0.433	Bed expansion (cm)	1.5, 3
Ø	1		
400~600 µm (medium)			
Mean particle size (µm)	496	Solid density (kg/m^3)	2485
Air velocity (m/s)	0.22~0.31	Bulk density (kg/m^3)	1600
u_{mf} (m/s, theoretical)	0.20	Bed height (cm)	28, 35
ε_{mf}	0.378, 0.374	Bed expansion (cm)	1, 1
Ø	1		
750~1000 µm (large)			
Mean particle size (µm)	933	Solid density (kg/m^3)	2485
Air velocity (m/s)	0.38~0.45	Bulk density (kg/m^3)	1630
u_{mf} (m/s, theoretical)	0.71	Bed height (cm)	28, 35
ε_{mf}	0.388, 0.38	Bed expansion (cm)	2, 2
Ø	1		

Table 4.2: Experimental set-up and parameters

Furthermore, some mixtures are made up by using existed particles with different ratios and components are also tested here with the same setup. The mean diameters of those mixtures are referred to one of the three groups of particles tested earlier, so as to study the bed behaviors under the conditions of same mean diameters but diverse components. The details are listed in Table 4.4:

Mixture 1: 41% large particle, 59% small particle			
Mean particle size (μm)	484	Bed expansion (cm)	2
Air velocity (m/s)	0.134	Solid density (kg/m^3)	2485
Bed height (cm)	28		
Mixture 2: 29% small particle, 50% medium particle, 21% large particle			
Mean particle size (μm)	488	Bed expansion (cm)	2
Air velocity (m/s)	0.1~0.23	Solid density (kg/m^3)	2485
Bed height (cm)	28		
Mixture 3: 43% small particle, 25% medium particle, 32% large particle			
Mean particle size (μm)	488	Bed expansion (cm)	2
Air velocity (m/s)	0.12~0.25	Solid density (kg/m^3)	2485
Bed height (cm)	28		

Table 4.3: Detailed parameters of experiments of testing mixers

Due to the potential of imperfectly mixing of the mixtures, the bulk densities for mixtures are not measured. But it is expected that the range of bulk densities of mixtures are higher than large powder and lower than small powder, i.e., close to medium powder.

4.3 Procedure

The experiments are carried out in a big lab. Preliminarily, the setup needs to be tested to ensure the air can go upwards through the distributor uniformly. Besides, it is also important to check the flow meter as a purpose of making sure the number of air flow can display correctly. So as to get the good quality of the videos, some parameters of the video camera are essential to set in a right way before starting the experiments as well, such as the shooting distance, angle, brightness.

For each group of particles, experiments are conducted with increasing air flows and two bed heights. At first, the air flow is adjusted to reach the minimum fluidization, which means the bed is just at the critical point where the bubble would show up by just increasing the air flow very slightly. The air flow rate at this point is recorded as the experimental minimum fluidization velocity of this particle. Afterwards, the air flow would be raised stepwise to get different bed states, and meanwhile, the videos are taken

with a length 20~25 s for each state. For the mixtures, particles are pre-mixed and introduced into setup, and further pre-mixed in the bed with violent air flow again.

5. Results and analysis

Some experiments are selected for detailed analysis from each group of different powders, different bed heights and different flow conditions owing to the good quality of videos. The movie sequences are extracted to show the bubble behaviors within the fluidized bed. The two important indexes, bubble velocity and bubble size are the main focus of the analysis. Besides, the comparisons of experimental and computational results are presented in this chapter as well.

5.1 Minimum fluidization velocity

From experiments, the minimum fluidization velocity (u_{mf}) could be determined by adjusting the gas valve to make the bed reach the minimum fluidization. The gas flow rate shown on the flow-meter can be approximately recognized as the u_{mf} of this powder. The experimental values are compared with theoretical values calculated from Eq. 2.6 and 2.9. The experimental values are 0.13, 0.22, 0.37 m/s in 28 cm bed height and 0.14, 0.24, 0.37 m/s in 35 cm bed height. The theoretical values are 0.0192, 0.192 for small, medium powder from Eq. 2.9 and 0.482 m/s for large particle from Eq. 2.6. The results are shown in Figure 5.1.

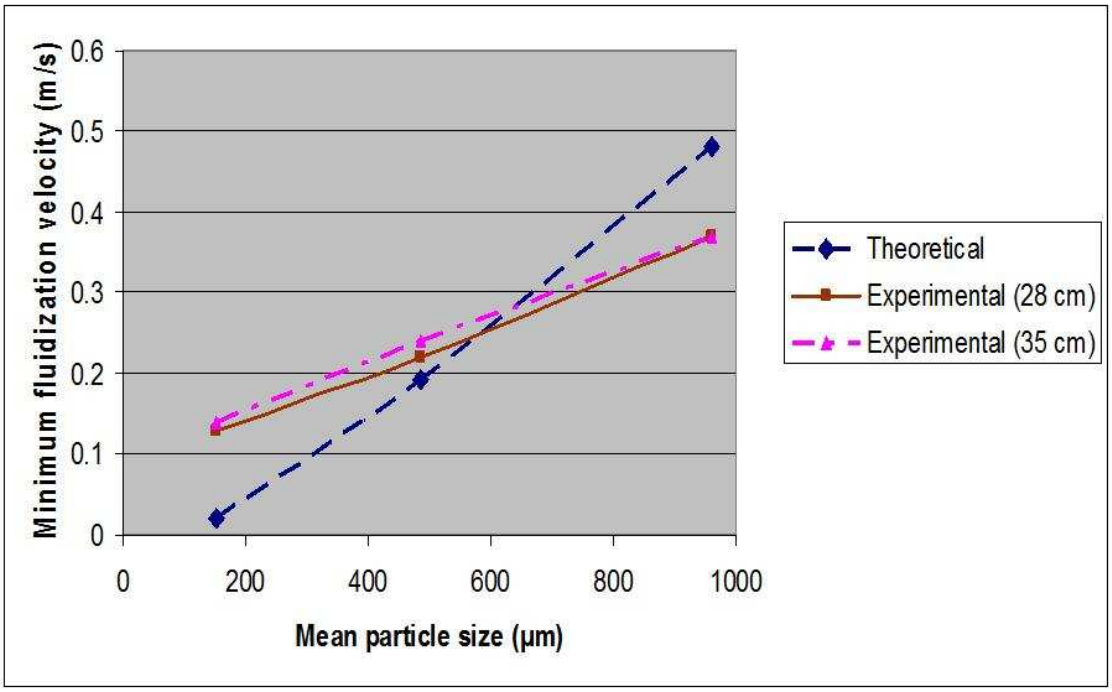

Figure 5.1: Comparison of the u_{mf} from experiments and theories for three particles.

According to Figure 5.1, u_{mf} is to rise with the increase of the particle size. The values for small and large particles show large discrepancies from theoretical values. The u_{mf} for medium particle agrees well with the theoretical value. The reason could probably be that

medium particle is more close to a typical group B particle, for which the equations are more applicable.

5.2 Small, medium and large particles

Three kinds of particles with different particle size distribution are used as operating particles. Based on visible experimental data, bubble shape, bubble velocity and bubble size are investigated in this section.

5.2.1 Movie sequences

Three experiments of different particles are selected typically for detailed analysis. From movie sequences below, it can be seen that the bubbles have different behaviors on size and shape in different beds of particles due to their intrinsic properties.

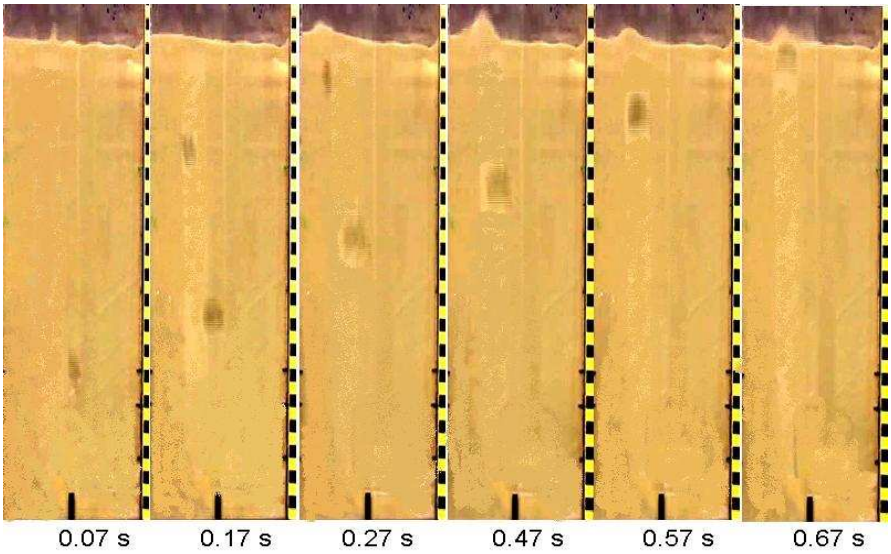

Figure 5.2: Movie sequence of the bed of small particles. The bed height is 35 cm, the superficial gas velocity is 0.15 m/s.

It can be seen in Figure 5.2, the bubble size and shape do not change too much during its movement. The bubble is small and kept elliptical. It takes around 0.6 s for the bubble to move from the position where it is first clearly observed to top of the bed.

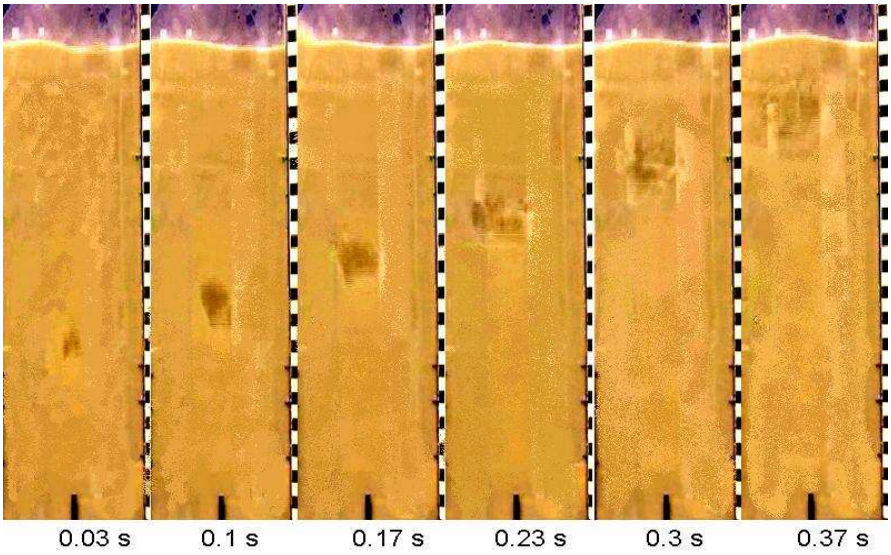

Figure 5.3: Movie sequence of the bed of medium particles. The bed height is 35 cm, the superficial gas velocity is 0.26 m/s.

As shown in Figure 5.3, the bubble is observed at the similar position to the bubble in small particle bed. It changes significantly on size and shape. It grows from a very small one into a big one, which is turbulent and tend to break up as it reaches the top. The time taken from the first position to the top is less than the one in small particle bed, which is around 0.34 s.

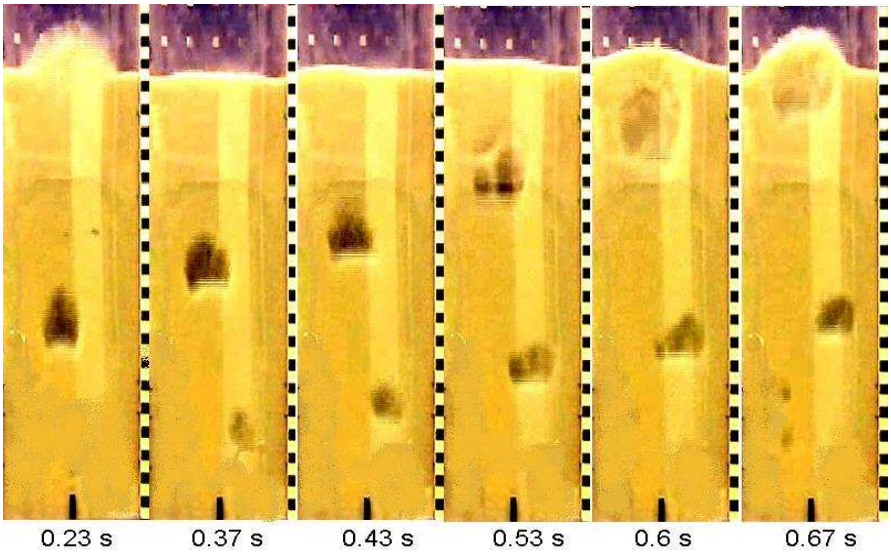

Figure 5.4: Movie sequence of the bed of large particles. The bed height is 35 cm, the superficial gas velocity is 0.42 m/s.

The bubble shown in Figure 5.4 has a similar tendency to the one in Figure 5.3. The bubble appears more clearly. It shows a tendency to split during its movement. The

bubble size also increases significantly when it approaches the top of the bed. Compared to small and medium particle beds, the interval between two bubbles is shorter. The time taken from the first position to the top is around 0.44 s.

As being observed, the bubble in small particle bed is much smaller than the ones in medium and large particle beds. When the bubbles approach the top, the ones in medium and large particle bed are clearly revealed with the behavior of breaking-up, which doesn't appear in small particle bed.

5.2.2 Bubble velocity

Based on the experimental videos, some properties can be analyzed in detail, such as bubble velocity, bubble size. Figure 5.5 to 5.7 show a common tendency on bubble velocity that it is in direct proportion of both the rising time (or the distance above the distributor, z), and the superficial gas velocity.

Many experiments are performed. The experimental videos are recorded and analyzed in order to investigate the bed behavior at different conditions. The bubble velocities are calculated manually by playing the experimental videos in Photron FASTCAM Viewer 2.4. The frame rate is 1/30. Since the experimental data distributes dispersedly, the trend line is used in Figure 5.5 to 5.7 to represent the main tendency of experimental data.

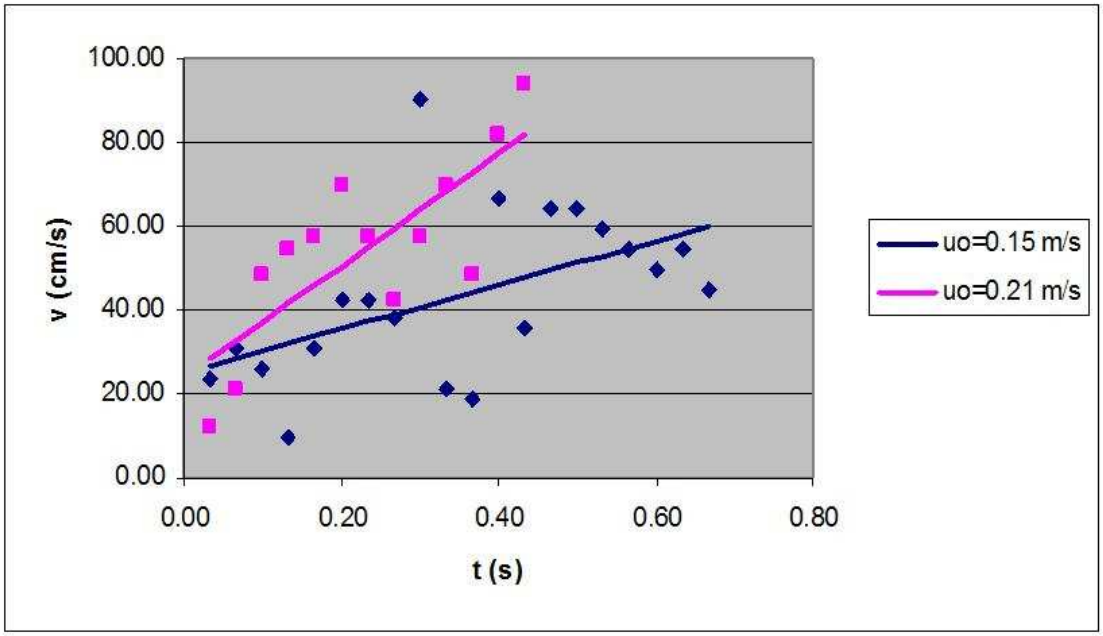

Figure 5.5: Change of bubble velocities with time for small particles. Bed height is 35 cm, u_o=0.15 and 0.21 m/s.

In Figure 5.5, the change in the superficial velocity u_o is 0.06 m/s. The bubble velocity at u_o=0.15 m/s increases from 26 cm/s to 60 cm/s, when the one at u_o=0.21 m/s rises from 27 cm/s to 82 cm/s.

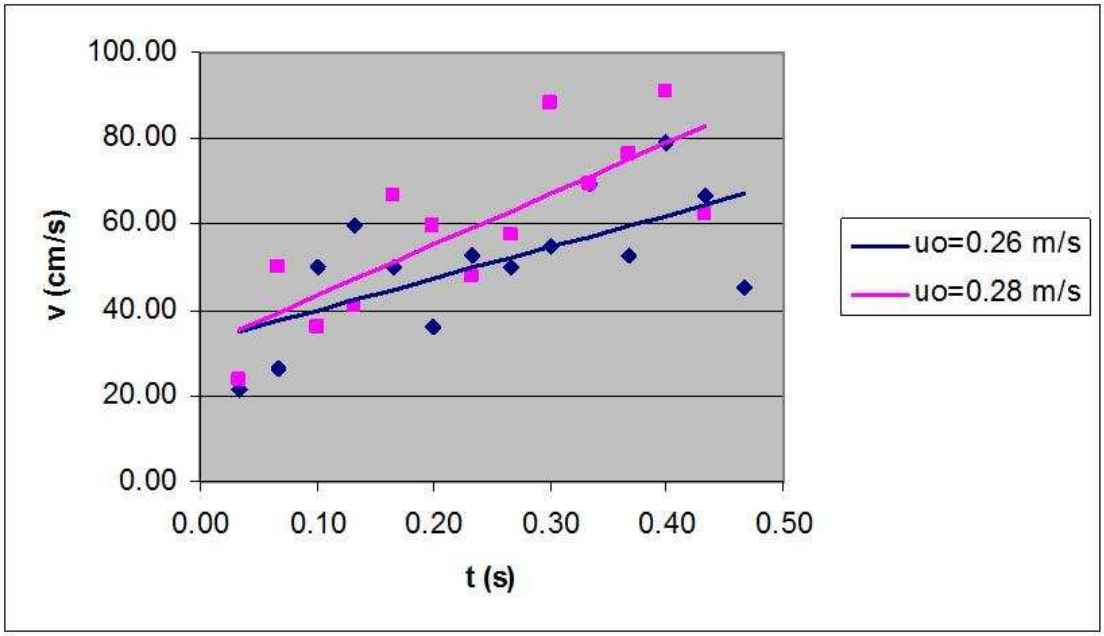

Figure 5.6: Change of bubble velocities with time for medium particles. Bed height is 35 cm, u_o=0.26 and 0.28 m/s.

In Figure 5.6, the change in the superficial velocity u_o, 0.02 m/s, is less than that in Figure 5.5. The bubble velocity at u_o=0.26 m/s starts from 35 cm/s to 68 cm/s, the one at u_o=0.28 m/s is from 35 cm/s to 82 cm/s.

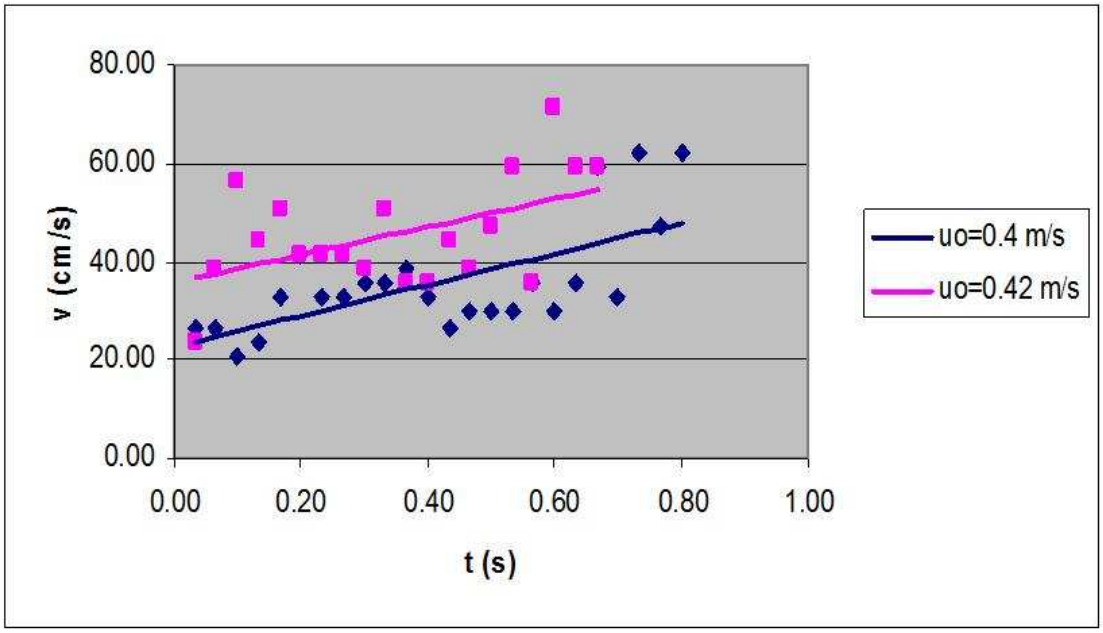

Figure 5.7: Change of bubble velocities with time for large particles. Bed height is 35 cm, u_o=0.4 and 0.42 m/s.

For large particle in Figure 5.7, the bubble velocity at u_o=0.4 m/s increases from 23 cm/s to 48 cm/s, the one at u_o=0.42 m/s is from 38 cm/s to 55 cm/s.

As apparently shown in Figure 5.5, 5.6 and 5.7, the bubble velocities appear sharp deviations at varied gas superficial velocities. The maximum of this deviation is correlated with the difference of used superficial velocities. Due to Figure 5.5 and 5.6, this deviation increases significantly with the height in the bed. The deviation between bubble velocities for superficial velocity 0.15 and 0.21 increases with the bed height and reaches the maximum at the top of the bed, which is around 20 cm/s. The same tendency can be observed in Figure 5.6. The reasons may be that the bubble is accelerated during its movement by the input fluid. In Figure 5.7, this deviation is kept almost constant.

The average bubble velocity is one output from the analysis on the experimental videos. The average velocity is calculated by using the height from where the bubble is firstly observed to the top of the bed, divided by the time consumed during the movement. This calculation is made for three powders apart. Figure 5.8 reveals variation of average bubble velocity with increasing superficial gas velocity at 28 cm bed height.

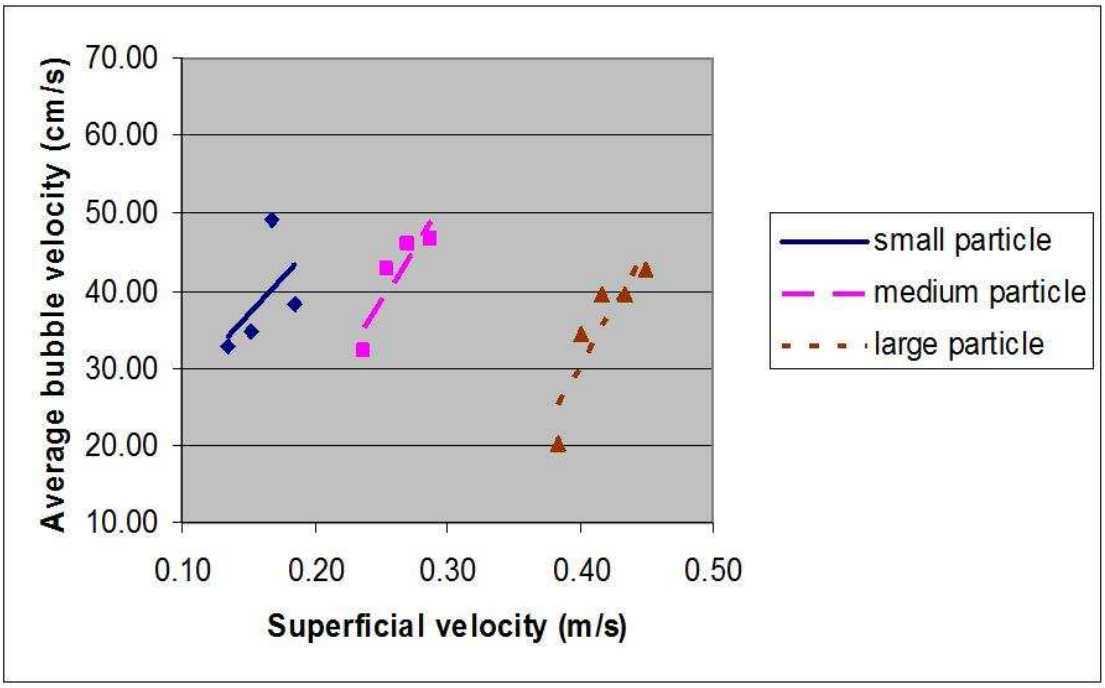

Figure 5.8: Change of average bubble velocity with superficial gas velocity for three powders. Bed height is 28 cm.

In Figure 5.8, the average velocities for three powders tend to increase with the increasing superficial gas velocity within their own ranges. It can be observed that average bubble velocities for three particles are approximately concentrated within a range, from 25 to 50 cm/s, even though the superficial velocities vary dramatically. Those three trend lines are approximately parallel, which means the accelerations are almost the same. The large particle has a lowest limitation of average velocity 20 cm/s, the small particle reaches the maximum average velocity at around 50 cm/s. It can therefore be preliminarily concluded that the bubble velocity is a function of height in the bed and superficial velocity.

5.2.3 Bubble size

The bubble size and shape also change with the distance above the distributor. Figure 5.9, 5.10 and 5.11 show the experimental and theoretical bubble sizes. The theoretical bubble size is calculated from Eq. 2.15. The experiments selected for analysis are in accordance with the ones in analysis of the velocity.

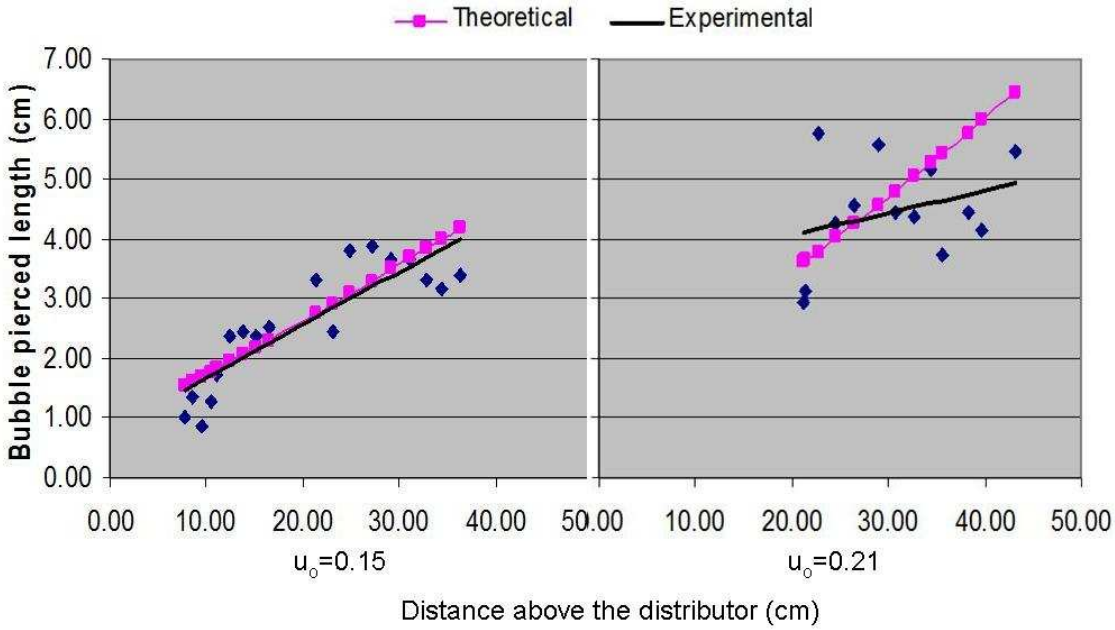

Figure 5.9: Change of bubble size with distance above the distributor for small particle. Bed height is 35 cm, u_o=0.15 and 0.21 m/s.

From Figure 5.9, it seems the variation of the superficial velocity has a strong effect on the bubble size. At u_o=0.15 m/s, the experimental bubble pierced length changes from 0.8 cm to 4 cm. which fits calculated values well. At u_o=0.21 m/s, the range of the bubble size is from 2.9 to 5.9 cm in experiments, and the points are getting too dispersive to suit the theory.

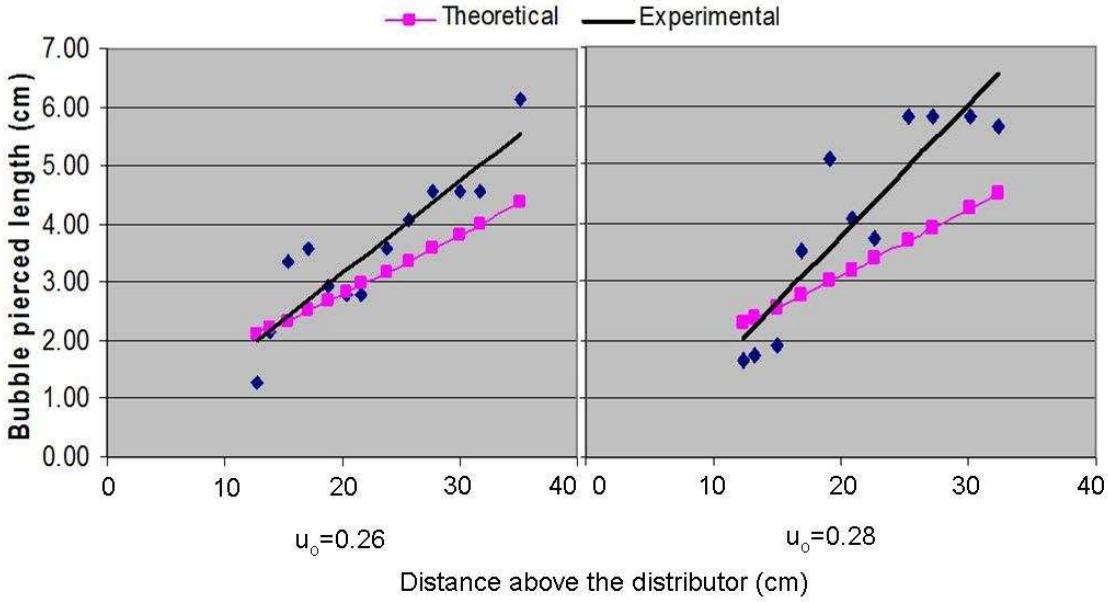

Figure 5.10: Change of bubble size with distance above the distributor for medium particle. Bed height is 35 cm, u_o=0.26 and 0.28 m/s.

Figure 10 shows the bubble size is a function of the bed height for medium particles. It is observed that the bubble size increases faster with the increasing superficial velocity. Bubble sizes range from 1.2 to 6.1 cm for u_o=0.26 m/s, and from 1.6 to 6 cm for u_o=0.28 m/s. This may be due to the small difference of the superficial velocities, 0.02 m/s. The experimental data fits the theory very well at low in the bed, and deviates from each other with the increasing height in the bed. But they still have similar trend.

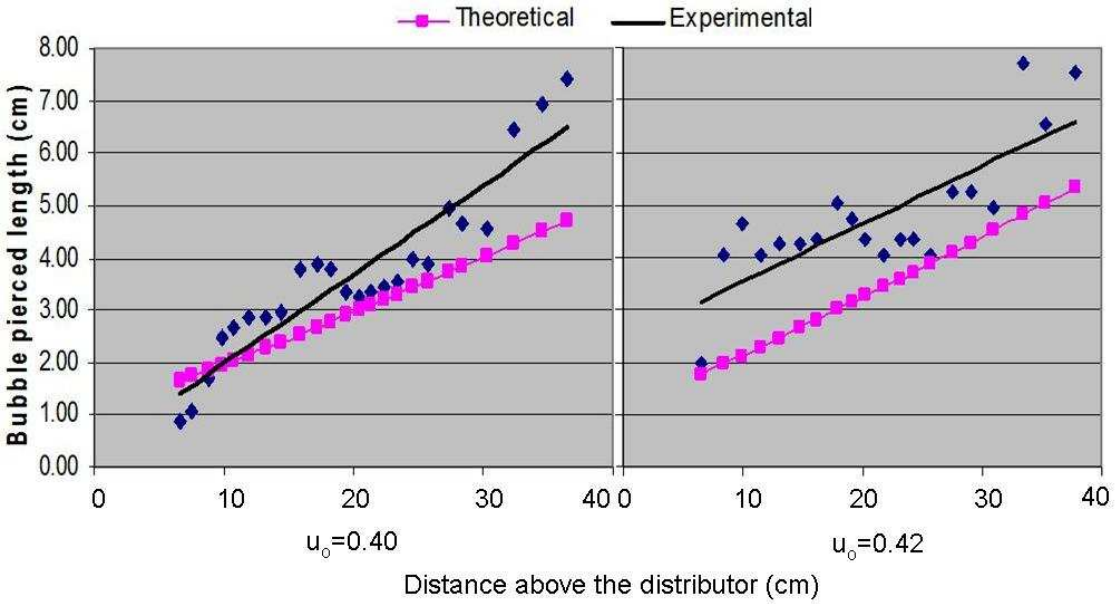

Figure 5.11: Change of bubble size with distance above the distributor for large particle. Bed height is 35 cm, u_o=0.40 and 0.42 m/s.

Figure 11 shows the bubble size is a function of the bed height for large particles. The situation in Figure 5.11 is similar to that in Figure 5.10. When u_o=0.42 m/s, experimental values are always beyond theoretical ones, and concentrate mostly within 4 to 5.5 cm. The range is from 2 to 7.8 cm. Experimental values with u_o=0.40 m/s are more consistent with the theory, and rise from 0.8 to 7.5 cm.

The results with small and medium particles represent good consistency with theory. The measured bubble sizes from the experiment with large particles show significant discrepancy from the calculated bubble size as shown in Figure 5.11. The reason may be that the operating conditions significantly exceed limitations within which the Eq. 2.15 can be applicable. But still, it also shows a similar tendency of theoretical result for large particle bed. From all three figures above, it can be found that bubble size is proportional of the distance above the distributor, z, and also affected by the variation of the superficial velocity.

5.3 Experimental and computational study on mixtures of particles

As a contribution to computational study of bubbling fluidized bed, experiments with mixtures of different powders are performed. It is very important to investigate the behavior of mixtures with different size distribution but same mean particle size, especially for the simulation. The size distribution of powders must be taken into consideration seriously when a simulation model is constructed for the fluidized bed. The incorrect selection of particle size may give rise to a completely deviated output, and further lead to a total uselessness of the whole simulation.

The details about the mixtures are presented in chapter 4. The three different mixtures used, have the same mean particle size, 484 µm, as the medium powder. Mixture 1 consists of 41% large particle, 59% small particle, mixture 2 is made up by 29% small particle, 50% medium particle, 21% large particle, mixture 3 is constituted by 43% small particle, 25% medium particle, 32% large particle. It can be therefore expected that the segregation may occur in beds of mixtures.

From Figure 5.12, 5.13 and 5.14, it is easily seen that the mixtures behave in a significant different way than the medium particle does, even thought they have same mean particle size.

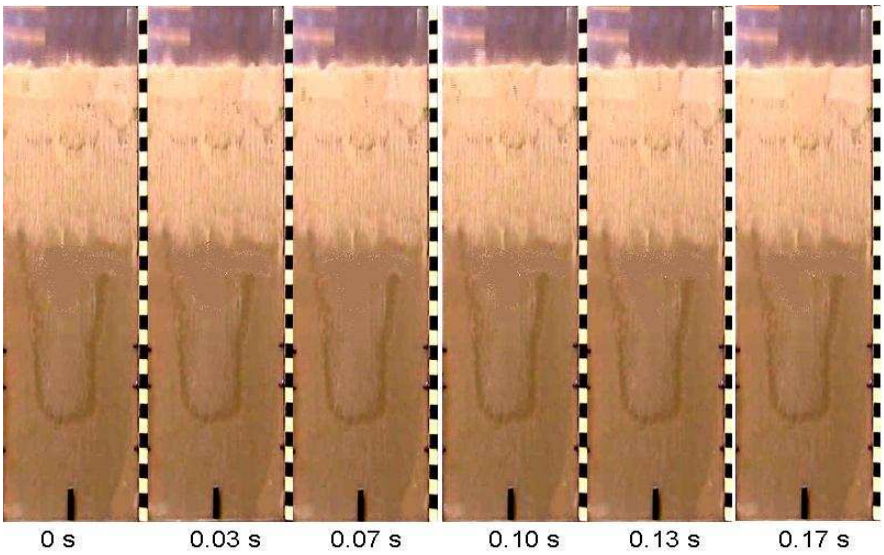

Figure 5.12: Movie sequence of the bed of mixture 1. The bed height is 28 cm, the superficial gas velocity is 0.134 m/s.

It can be seen in Figure 5.12 that a sharp segregation shows up at the upper part around the middle of the bed. There is not clear bubbles observed, instead, turbulence occurs in the upper part.

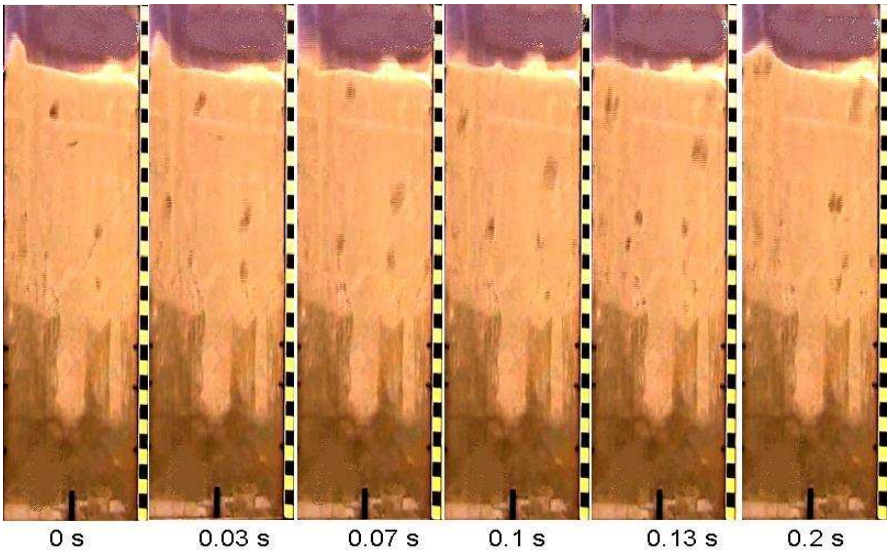

Figure 5.13: Movie sequence of the bed of mixture 2. The bed height is 28 cm, the superficial gas velocity is 0.134 m/s.

In Figure 5.13, some channels occur at the lower part of the bed, bubbles with small size rise from these channels to the top.

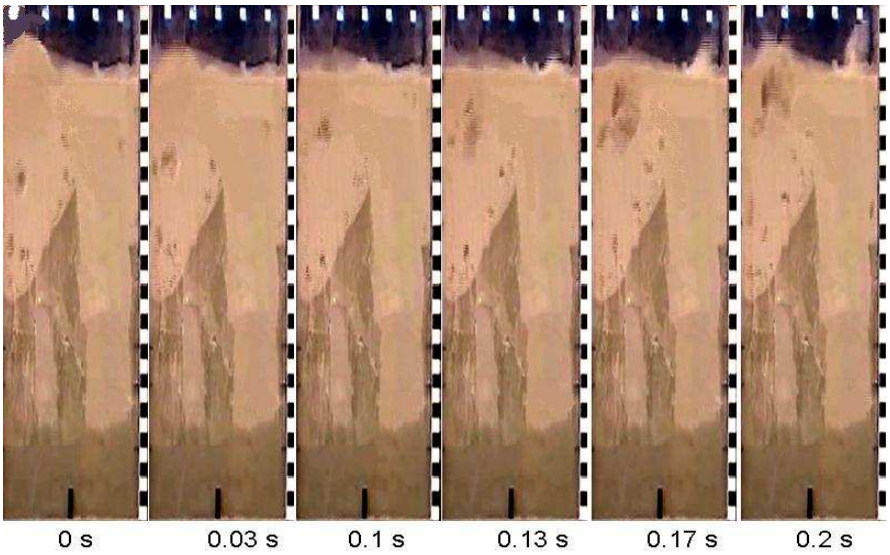

Figure 5.14: Movie sequence of the bed of mixture 3. The bed height is 28 cm, The superficial gas velocity is 0.134 m/s.

The channels in Figure 5.14 are at the similar position, but longer than the ones in mixture 2. Larger bubbles appear in the bed of the mixture 3.

From the figures above, very sharp segregations of particles can be observed in all three beds. Besides, there appear channels apparently at the middle regions between larger and

smaller particles. Bubbles show up in upper region mostly through channels from the bottom of beds. There are not bubbles at the lower layers and rarely at the layer between. It is supposed to be that the small, medium and large particles are taking the dominance of particle mixtures at upper, middle and lower layer, and decide the bubble behaviors mainly.

Even though the three mixtures have the same mean size, and behave in close way as described above, they still have some discrepancies in details, for example, the shape of channels, the thickness of layers and the bubble behaviors. It seems the behaviors of beds have strong correlation with the composition of particles, not only the mean particle size. Several simulations with same particles and operating parameters are performed by D. G. A. S. U. Ariyarathna at Telemark University College, Norway, and made comparisons to testify with the experimental results of the mixture 1 and 2.

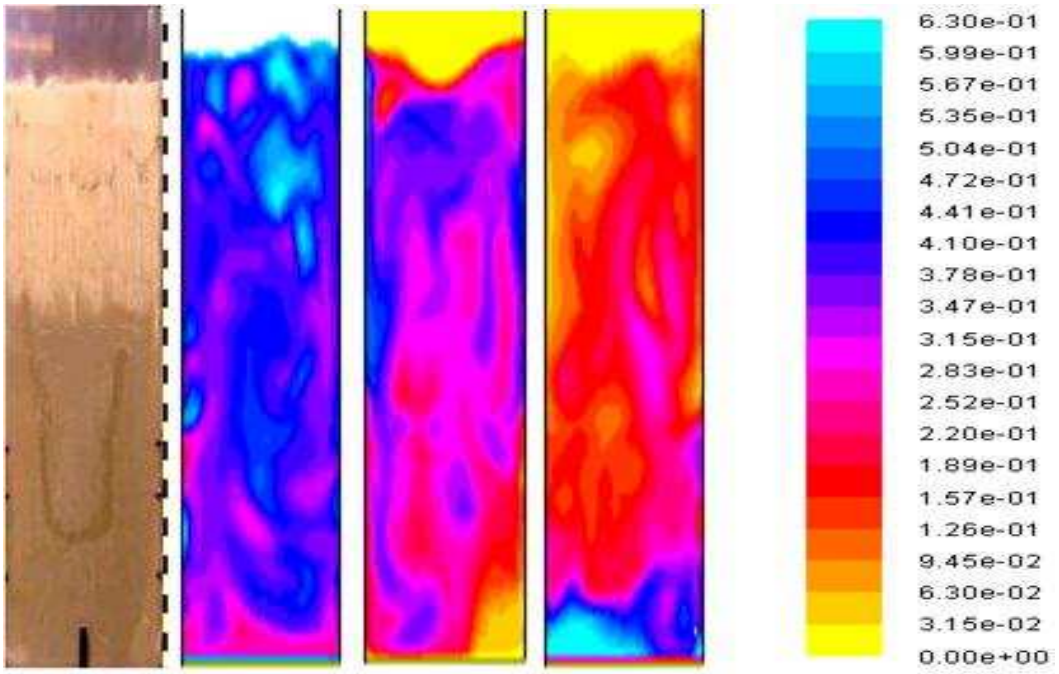

Figure 5.15: Comparison of the experimental and computational results for mixture 1.

According to Figure 5.15, the gas fraction is seen mainly at the upper layer of the bed, bubbles therefore occur mostly there, the distribution of bubbles are uniform in that part. Small particles are also kept at the top more often, when large particles take the predominance at the bottom of the bed.

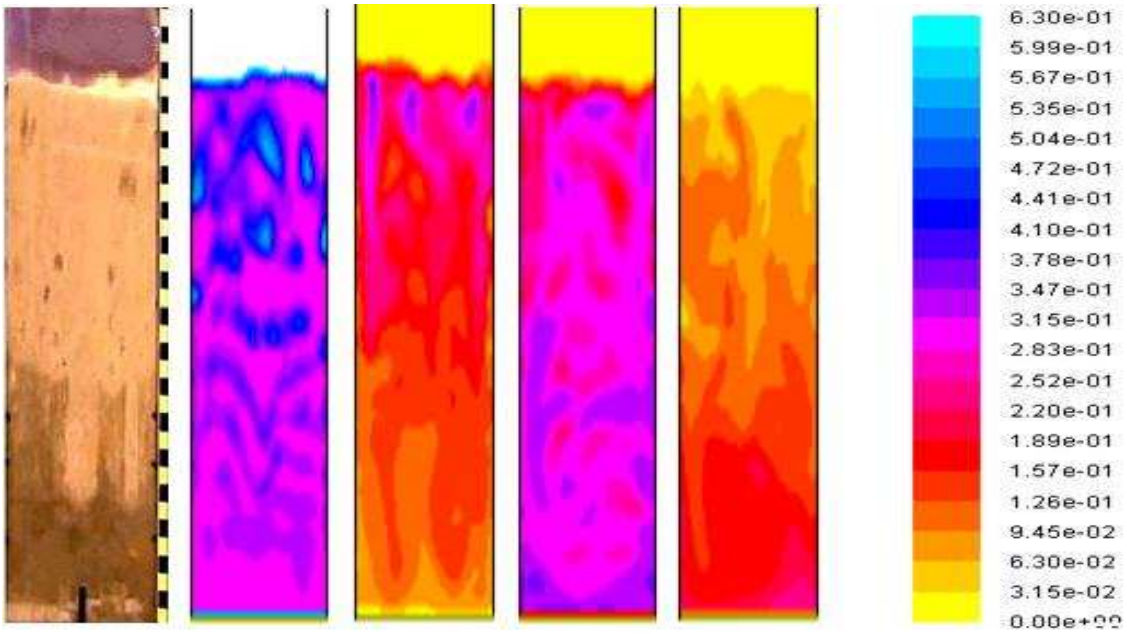

Figure 5.16: Comparison of the experimental and computational results for mixture 2.

The contours of gas fraction in Figure 5.16 show a significantly concentrated distribution of bubbles mainly at upper part of the bed. Every single segment of the gas fractions is sharp and separate, which may lead to obvious bubble in the bed. Small and large particles have similar behaviors as analyzed for mixture 1 in Figure 5.15. The only deviation is that their dispersions are more uniform than in mixture 1. Medium particles have uniform distribution. They mostly centralize at the middle region of the bed. Meanwhile, a few of them disperse at the upper and lower portion of bed which are mixed with small and large particles respectively.

By checking Figure 5.15 and 5.16, it can be found that the bed behaviors revealed in simulations fit the experimental data well. The total behaviors can be summarized as: sharp segregations occur in beds of mixtures; distributions of particles are divided into three layers; large particles normally stay at the bottom of the bed, while small and medium particles disperse to upper and middle regions respectively; in each region, the bed consists of three particles together, but one of them predominates in volume fraction. From both the experiments and simulations, it can be realized that the behavior of medium particle bed is neither like mixture 1 nor mixture 2, even though they have the same mean particle size. The size distribution decides the main behavior of beds in some degree.

5.4 Coalescence and Splitting

According to Kunii and Levenspiel (1991), the coalescence and splitting can be explained generally as interaction of adjacent bubbles. The consequence of coalescence and splitting is that the maximum bubble size may occur in the bed. This phenomenon is emerged in experiments and simply shown in Figure 5.17 and 5.18.

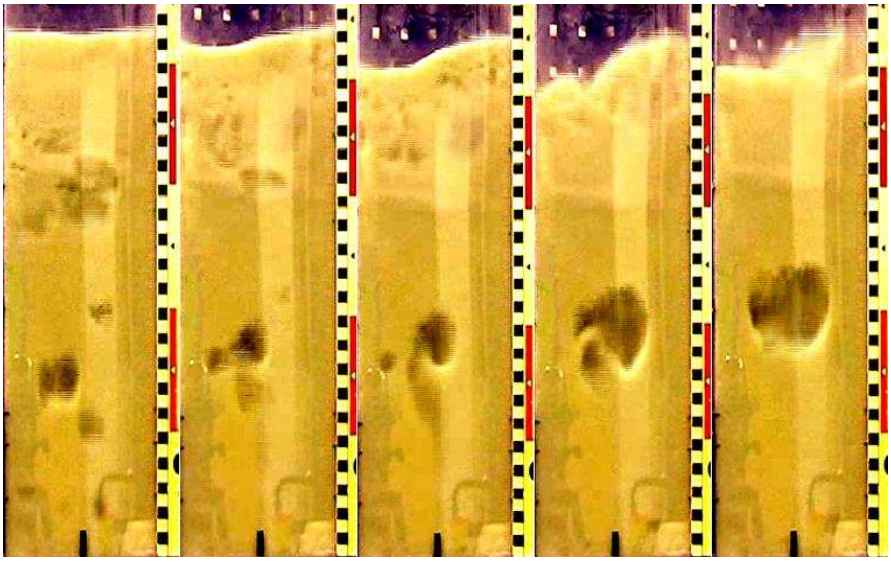

Figure 5.17: Movie sequence of bubble coalescence (large powder).

Figure 5.17 shows a coalescence of two vertical bubbles. This kind of coalescence frequently occurs in lower portion of beds supported by perforated plate distributors as described in Kunii and Levenspiel's study.

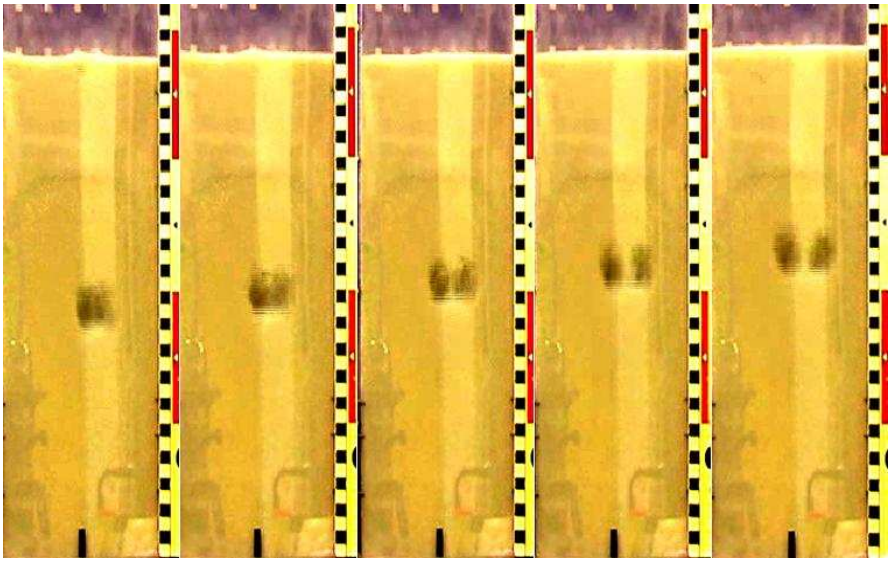

Figure 5.18: Movie sequence of bubble splitting. (large powder).

Figure 5.18 shows that an obvious fission is firstly developed downward at the roof of the bubble, and then grows rapidly to cause the bubble to split vertically, which fits what are observed by Rowe (1971) well.

6. Conclusions

The performance of bubbling fluidized bed depends strongly on the bubble behavior. There are many factors that may influence how bubbles behave in the bed, such as particle properties, design of the bubbling bed, flow conditions. A 2-D fluidized bed with dimension 0.8 m (height) × 0.2 m (width) × 0.025 m (depth) is constructed. The experiments are run with varied powders and flow conditions. Three powders, with range from less than 63 µm to more than 1000 µm, are used as working powders, mixtures consisted of different composition of three powders are also tested, which have the same mean diameter as medium particle. The applied flow rates range from 0.13 to 0.45 m/s. The visible experimental data are analyzed and compared with computational results performed by G. A. S. U. Ariyarathna at Telemark University College, 2008. The analysis mostly focus on minimum fluidization velocity, bubble velocity, bubble size, and use the experimental visible data to testify with simulation pictures in order to investigate the effects of particle size distribution on bubble behaviors of bubbling fluidized bed. Based on the analysis, some important conclusions could be made.

The minimum fluidization velocity (u_{mf}) is to rise with the increase of the particle size. Those values of small and large particles show significant difference from theoretical values, the value of medium particle agrees well with the theoretical value. The reason can probably be that medium particle is more close to a typical group B particle, for which the theories are more applicable. Three experiments of different particles are selected typically for detailed analysis. In movie sequences extracted from visual experimental data, it can be obviously seen that bubbles have different behaviors on size and shape in different beds of particles due to their intrinsic properties, even thought the operating conditions are similar.

A common tendency is revealed on bubble velocity that it changes with different distance above the distributor and the superficial velocities. The bubble velocities also appear sharp deviation at varied gas superficial velocities, which can reach maximum 20 cm/s within testing range. Furthermore, this deviation has an increasing tendency with the increase of gas superficial velocity. It can be concluded that the bubble velocity is a function of the height in the bed and the superficial velocity.

The bubble shape also changes with time, or more accurately, with the distance above the distributor, since it can be represented as a function of time. Bubble size is proportional of the distance above the distributor, z, as well.

The mixtures behave in a significant different way than the medium particle does, even thought they have same mean particle size. The computational studies show the parallel results. Very sharp segregations of particles can be seen in all three beds. Besides, there appear channels apparently at the middle regions between larger and smaller particles. The bed behaviors revealed in simulations fit the experimental videos well. The total behaviors can be summarized as: Sharp segregations occur in beds of the mixtures. Distributions of particles are divided into three layers generally. Large particles normally stay at the bottom of the bed, while small and medium particles disperse to upper and

middle regions respectively. In each region, the bed is consisted of three particles together, but one of them predominates in volume fraction. As concluded above, behaviors of beds have a strong correlation with the size distribution of particles, not only the mean particle size.

Bibliography

Baddour, Carole E. and Briens, Cedric (2005), Carbon Nano-tube Synthesis: A Review, *International Journal of Chemical Reactor Engineering*, **3**: R3.

Beck, M.S., Campogrande, E., Morris, M., Williams, R.A., Waterfall, R.C. (1993), Tomographic Techniques for Process Design and Operation, Computational Mechanics Publications, Southampton, UK.

Chen, R.C., Fan, L.S. (1992), Particle image velocimetry for characterizing the flow structure in three-dimensional gas–liquid–solid fluidized beds, *Chem. Eng. Sci.*, **47**, pp. 3615-3622.

Gamblin, B., Newton, D., Grant, C. (1993), X-ray characterization of the gas flow patterns from FCC regenerator air ring nozzles, in: A.A. Avidan, Circulating Fluidized Bed Technology IV, Proc. 4th Int. Conf. Circulating Fluidized Beds, SomersetrPa., USA, pp. 494-499.

Geldart, D., Abdullah, E.C., Hassanpour, A., Nwoke, L.C., Wouters, I. (2006), Characterization of powder flowability using measurement of angle of repose. *China Particuology*, **4(3-4)**, pp. 104-107.

Gidaspow, D. (1994), Multiphase Flow and Fluidization. Academic Press, Boston.

Halow, J.S., Fasching, G.E., Nicoletti, P., Spenik, J.L. (1993), Observations of a fluidized bed using capacitance imaging, *Chem. Eng Sci.* **48**, pp. 643-659.

Holoboff, J., Kantzas, A., Kalogerakis, N. (1995), Utilization of computer assisted tomography in the determination of the spatial variability of voidage in a gas–solid fluidized bed, in: J.F. Large, Fluidization VIII, 8th Int. Engineering Foundation Conference on Fluidization, preprints, Tours, France, pp. 295-302.

Horio, M., Kuroki, H. (1994), Three-dimensional flow visualization of dilutely dispersed solids in bubbling and circulating fluidized beds, *Chem. Eng. Sci.* **49**, pp. 2413-2421.

Horio, M., Nonaka, A. (1987), A Generalized Bubble Diameter Correlation for Gas-Solid Fluidized Beds. *AIChE Journal*, **33(11)**, pp. 1865-1872.

Huang, S.M., Xie, C.G., Thorn, R., Snowden, D., Beck, M.S. (1992), Design of sensor electronics for electrical capacitance tomography, IEE Proceedings **6**, **139**, pp. 83-88.

Internet source: http://en.wikipedia.org/wiki/Fluidization

Internet source: http://en.wikipedia.org/wiki/Fluidized_bed

Kantzas, A., Kalogerakis, N. (1996), Monitoring the fluidization characteristics of polyolefin resins using X-ray computer assisted tomography scanning, *Chem. Eng. Sci.* **51**, pp. 1979-1990.

Kunii, D., Levenspiel, O. (1991), Fluidization Engineering. Second edition, Butterworth-Heineman series in chemical engineering.

Kuroki, H., Horio, M. (1993), The flow structure of a three-dimensional circulating fluidized bed observed by the laser sheet technique, in: A.A. Avidan, Circulating Fluidized Bed Technology IV, Proc. 4th Int. Conf. Circulating Fluidized Beds, SomersetrPa., USA, pp. 77-84.

Li, H., Xia Y., Tung, Y., Kwauk, M. (1991), Micro-visualization of two-phase structure in a fast fluidized bed, in: P. Basu, M. Horio, M. Hasatani, Circulating Fluidized Bed Technology III, Pergamon, Oxford, pp. 183-188.

Lischer, D.J., Louge, M.Y. (1992), Optical fiber measurements of particle concentration in dense suspensions: calibration and simulation, Applied Optics **31**, pp. 5106-5113.

Louge, M., Experimental techniques, in: J. Grace, T. Knowlton, A.A. Avidan, Circulating Fluidized Beds, Chap. 9, Chapman & Hall, London, 1996.

Reh, L., Li, J. (1991), Measurement of voidage in fluidized beds by optical probes, in: P. Basu, et al. (Eds.), Circulating Fluidized Bed Technology III, Pergamon, New York, pp. 163-170.

Rensner, D., Werther, J. (1993), Estimation of the effective measuring volume of single-fiber reflection probes for solid volume concentration measurements, Part. Part. Syst. Charact. **10**, pp. 48-55.

Rhodes, M.J. (1990), Principles of Powder Technology. John Wiley & Sons Ltd.

Rix, S.J.L., Glass, D.H., Greated, C.A. (1996), Preliminary studies of elutriation from gas fluidized beds using particle image velocimetry, *Chem. Eng. Sci.* **51**, pp. 3479-3489.

Seville, J.P.K., Simons, S.J.R., Broadbent C.J., Martin, T.W., Parker, D.J., Beynon, T.D. (1995), Particle velocities in gas-fluidized beds, in: J.F. Large, Fluidization VIII, 8th Int. Engineering Foundation Conf. on Fluidization, preprints, Tours, France, pp. 319-326.

Seville, J.P.K., Willett, C.D., & Knight, P.C. (2000). Inter-particle forces in fluidization: A review. *Powder Technology*, **113**, pp. 261-268.

Simons, S.J.R. (1995), Imaging techniques for fluidized bed systems: a review. *The Chemical Engineering Journal*, 56, pp. 83-93.

Werther, J. (1999), Measurement techniques in fluidized beds. *Powder Technology*, **102**, pp. 15-36.

Werther, J., Hage, B., Rudnick, C. (1996), A comparison of laser doppler and single-fiber reflection probes for the measurement of the velocity of solids in a gas–solid circulating fluidized bed, *Chem. Eng. Proc.* **35**, pp. 381-391.

Werther, J., Hartge, E.-U., Rensner, D. (1993), Measurement techniques for gas–solid fluidized bed reactors, Int. *Chem. Eng.* **33**, pp. 18-27.

Wirth, K.E., Seiter, M. (1991), Solids concentration and solids velocity in the wall region of circulating fluidized beds, in: E.J. Anthony, Proc. 11th Int. Conf. Fluidized Bed Combustion, ASME, New York, pp. 311-315.

Wong, A.C.-Y. (2002). Characterization of the flowability of glass beads by bulk densities ratio. *Chemical Engineering Science*, **55**, pp. 3855-3859.

Wong, A.C.-Y. (2002). Use of angle of repose and bulk densities for powder characterization and the prediction of minimum fluidization and minimum bubbling velocities. *Chemical Engineering Science*, **57**, pp. 2635-2640.

Xie, C.G., Huang, S.M., Hoyle, B.S., Thorn, R., Lenn, C., Snowden, D., Beck, M.S. (1992), Electrical capacitance tomography for flow imaging: system model for development of image reconstruction algorithms and design of primary sensors, IEE Proceedings **6**, **139**, pp. 89-98.

Yeung, S.L.S. (1995). Evaluation of the flowability of powders of different size and shape. B. Eng. thesis. The University of Hong Kong.

Zhang, W., Tung, Y., Johnsson, F. (1991), Radial voidage profiles in fast fluidized beds of different diameters, Chem. Eng. Sci. **46**, pp. 3045-3052.

Zheng, Z., Zhu, J., Grace, J.R., Lim, C.J. (1992), Brereton, C.H.M., Particle motion in circulating and revolving fluidized beds via microcomputer-controlled color-stroboscopic photography, in: O.E. Potter, D.J. Nicklin, Fluidization VII, Proc. 7th Int. Engineering Foundation Conf. Fluidization, Engineering Foundation, New York, pp. 781-789.

Nomenclature

A	cross-sectional area of the column [m^2]
A	y offset
AOR	angle of repose [-]
B	amplitude
C	decay constant [-]
d_b	diameter of bubble [m]
d_i	Arithmetic mean of adjacent sieves [-]
d_p	mean particle size [µm]
d_t	diameter of the bed [m]
g	acceleration of gravity, =9.8 m/s^2
H	average bed height at velocity U [m]
H_{mf}	bed height at velocity U_{mf} [m]
HR	Hausner ratio [-]
H_s	height of the gently settled bed [m]
M_Bg	submerged weight of the bed [-]
$Ø_s$, ϕ_s	gas/particle drag coefficient [$kg/m^3 \cdot s$]
Q_B	volumetric flow rate of bubbles [m^3/h]
Re	Reynolds number [-]
U_B	average bubble velocity [m/s]
u_b	bubble velocity [cm/s]
u_{br}	rise velocity of single bubbles [m/s]
u_{mb}	minimum bubbling velocity [m/s]
u_{mf}, U_{mf}	minimum fluidization velocity [m/s]
u_o	superficial velocity [m/s]
V_{bulk}	volume of particles within the bed [m^3]
$V_{m, bulk}$	volume of particles within the bed at minimum fluidization [m^3]
x_i	mass fraction [-]
z	distance above the distributor [cm]
ε_{mf}	volume fraction at minimum fluidization [-]
ρ_A	aerated bulk density [kg/m^3]
ρ_{ABS}	true or absolute density [kg/m^3]
ρ_{BS}	bulk density of the gently settled bed [kg/m^3]
P_{bulk}	bulk density of particles within the bed [kg/m^3]
ρ_g, ρ_f	density of fluids [kg/m^3]
$\rho_{m, bulk}$	bulk density of particles within the bed at minimum fluidization [kg/m^3]
ρ_s	density of solids [kg/m^3]
ρ_T	tapped bulk density [kg/m^3]
µ	shear viscosity [$kg/m \cdot s$]

Appendix

A. Detailed properties for groups of particles

Group (Increasing size and density)		C	A	B	D
Most obvious characteristic		Cohesive, difficult to fluidize	Bubble-free range of fluidization	Starts bubbling at U_{mf}	Coarse solids
Typical solids \ property		Flour, cement	Cracking catalyst	Building sand, table salt	Crushed limestone, coffee beans
1. Bed expansion		Low when bed channels, can be high when fluidized	High	Moderate	Low
2. Deaeration rate		Initially fast, exponential	Slow, linear	Fast	Fast
3. Bubble properties		No bubbles. Channels, and cracks	Splitting/recoalescence predominate; maximum size exists; large wake	No limit on size	No known upper size; small wake
4. Solid mixing[a]		Very low	High	Moderate	Low
5. Gas back-mixing[a]		Very low	High	Moderate	Low
6. Slug properties		Solids slugs	Axisymmetric	Axisymmetric, asymmetric	Horizontal voids, solids slugs, wall slugs
7. Spouting		No	No, except in very shallow beds	Shallow beds only	Yes, even in deep beds.
Effect on properties 1 to 7 of:	Mean particle size within group	Cohesiveness increases as d_p decreases	Properties improve as size decreases	Properties improve as size decreases	Not known
	Particle size distribution[b]	Not known	Increasing <45 μm fraction improves properties	None	Increases segregation
	Increasing pressure, temperature, viscosity, density of gas	Probably improves	Definitely improves	Uncertain, some possibly	Uncertain, some possibly

a- At equal $U-U_{mf}$.
b- At equal d_p.

B. Measurements of particle size distribution for three groups

The particles are double vibrating with 10 min firstly and 5 min secondly, in total 15 min, to check the complete separation.

100~200 µm			400~600 µm			750~1000 µm		
Particle size (µm)	% of size by mass	Cumulative % of size by mass	Particle size (µm)	% of size by mass	Cumulative % of size by mass	Particle size (µm)	% of size by mass	Cumulative % of size by mass
0~63	0.09	0.09	0~300	0.35	0.35	0~500	0.03	0.03
63~106	9.44	9.53	300~355	2.45	2.8	500 ~630	0.02	0.05
106~150	42.18	51.01	355~425	22.53	25.33	630~710	0.04	0.09
150~200	46.16	97.87	425~500	47.62	72.95	710~850	24.1	24.19
200~250	2.12	99.99	500~630	26.74	99.69	850~1000	64.24	88.43
>250	0.01	100	>630	0.31	100	>1000	11.57	100